ISSN 2410-3462

Volume 9, Issue 27 – July – December - 2022

Journal Simulation and Laboratory

ECORFAN®

Journal Simulation and Laboratory, Volume 9, Issue 27, July - December 2021, is a journal edited six monthly by ECORFAN-Bolivia. 21 Loa 1179, Cd. Sucre. Chuquisaca, Bolivia. WEB: www.ecorfan.org, revista@ecorfan.org. Chief Editor: SERRANO-PACHECO, Martha. PhD. ISSN-On line: 2410-3462. Responsible for the latest update of this number ECORFAN Computer Unit. ESCAMILLA-BOUCHÁN, Imelda, PhD, LUNA-SOTO, Vladimir. PhD. Loa 1179, Cd. Sucre. Chuquisaca, Bolivia, last updated December 31, 2022.

Journal Simulation and Laboratory

Definition of Research Journal

Scientific Objectives

Support the international scientific community in its written production Science, Technology and Innovation in the Field of Biology and Chemistry, in Subdisciplines of movement, sound and energy, thermoelectricity, quantum phenomena, molecular biology, molecular biology of microorganisms, molecular biology of plants, microbiological chemistry, cellular morphology, general chemistry, quantum chemistry.

ECORFAN-Mexico SC is a Scientific and Technological Company in contribution to the Human Resource training focused on the continuity in the critical analysis of International Research and is attached to CONACYT-RENIECYT number 1702902, its commitment is to disseminate research and contributions of the International Scientific Community, academic institutions, agencies and entities of the public and private sectors and contribute to the linking of researchers who carry out scientific activities, technological developments and training of specialized human resources with governments, companies and social organizations.

Encourage the interlocution of the International Scientific Community with other Study Centers in Mexico and abroad and promote a wide incorporation of academics, specialists and researchers to the publication in Science Structures of Autonomous Universities - State Public Universities - Federal IES - Polytechnic Universities - Technological Universities - Federal Technological Institutes - Normal Schools - Decentralized Technological Institutes - Intercultural Universities - S & T Councils - CONACYT Research Centers.

Scope, Coverage and Audience

Journal Simulation and Laboratory is a Research Journal edited by ECORFAN-Mexico S.C in its Holding with repository in Bolivia, is a scientific publication arbitrated and indexed with semester periods. It supports a wide range of contents that are evaluated by academic peers by the Double-Blind method, around subjects related to the theory and practice of movement, sound and energy, thermoelectricity, quantum phenomena, molecular biology, molecular biology of microorganisms, molecular biology of plants, microbiological chemistry, cellular morphology, general chemistry, quantum chemistry with diverse approaches and perspectives, that contribute to the diffusion of the development of Science Technology and Innovation that allow the arguments related to the decision making and influence in the formulation of international policies in the Field of Biology and Chemistry. The editorial horizon of ECORFAN-Mexico® extends beyond the academy and integrates other segments of research and analysis outside the scope, as long as they meet the requirements of rigorous argumentative and scientific, as well as addressing issues of general and current interest of the International Scientific Society.

Editorial Board

Arbitration Committee

Assignment of Rights

The sending of an Article to Journal Simulation and Laboratory emanates the commitment of the author not to submit it simultaneously to the consideration of other series publications for it must complement the Originality Format for its Article.

The authors sign the Authorization Format for their Article to be disseminated by means that ECORFAN-Mexico, S.C. In its Holding Bolivia considers pertinent for disclosure and diffusion of its Article its Rights of Work.

Declaration of Authorship

Indicate the Name of Author and Coauthors at most in the participation of the Article and indicate in extensive the Institutional Affiliation indicating the Department.

Identify the Name of Author and Coauthors at most with the CVU Scholarship Number-PNPC or SNI-CONACYT- Indicating the Researcher Level and their Google Scholar Profile to verify their Citation Level and H index.

Identify the Name of Author and Coauthors at most in the Science and Technology Profiles widely accepted by the International Scientific Community ORC ID - Researcher ID Thomson - arXiv Author ID - PubMed Author ID - Open ID respectively.

Indicate the contact for correspondence to the Author (Mail and Telephone) and indicate the Researcher who contributes as the first Author of the Article.

Plagiarism Detection

All Articles will be tested by plagiarism software PLAGSCAN if a plagiarism level is detected Positive will not be sent to arbitration and will be rescinded of the reception of the Article notifying the Authors responsible, claiming that academic plagiarism is criminalized in the Penal Code.

Arbitration Process

All Articles will be evaluated by academic peers by the Double Blind method, the Arbitration Approval is a requirement for the Editorial Board to make a final decision that will be final in all cases. MARVID® is a derivative brand of ECORFAN® specialized in providing the expert evaluators all of them with Doctorate degree and distinction of International Researchers in the respective Councils of Science and Technology the counterpart of CONACYT for the chapters of America-Europe-Asia- Africa and Oceania. The identification of the authorship should only appear on a first removable page, in order to ensure that the Arbitration process is anonymous and covers the following stages: Identification of the Research Journal with its author occupation rate - Identification of Authors and Coauthors - Detection of plagiarism PLAGSCAN - Review of Formats of Authorization and Originality-Allocation to the Editorial Board- Allocation of the pair of Expert Arbitrators-Notification of Arbitration -Declaration of observations to the Author-Verification of Article Modified for Editing-Publication.

Instructions for Scientific, Technological and Innovation Publication

Knowledge Area

The works must be unpublished and refer to topics of movement, sound and energy, thermoelectricity, quantum phenomena, molecular biology, molecular biology of microorganisms, molecular biology of plants, microbiological chemistry, cellular morphology, general chemistry, quantum chemistry and other topics related to Biology and Chemistry.

Presentation of the content

In the first article we present, *Comparison of Vegsyst and Hortsyt models: Two models of growth of greenhouse crops* by MARTINEZ-RUIZ, Antonio, QUINTANAR-OLGUIN, Juan, SERVÍN-PALESTINA, Miguel and FLORES-DE LA ROSA, Felipe Roberto, with adscription in the Instituto Nacional de Investigaciones Forestales Agrícolas y Pecuarias, in the next article we present, *Control of a CNC laser engraver machine for non-metallic materials* by PACHECO-ALVARADO, Luis Kevin, GONZALEZ-MONZON, Ana Lilia, PIÑA-ALCANTARA Henry Christopher and TORRES-ARREOLA, León Guillermo, with adscription in the Tecnológico de Estudios Superiores de Jilotepec, in the next article we present, *Analysis of thermoelectrics used in the aerospace industry for power generation by the seebeck effect* by RODRIGUEZ-AVILA, Jesus, VALLE-HERNANDEZ, Julio and GALLARDO-VILLARREAL, José Manuel, with adscription in the Universidad Politécnica Metropolitana de Hidalgo and Universidad Autónoma del Estado de Hidalgo, in the next article we present, *Production of volatile compounds and lipopeptides as antagonistic mechanisms of two Bacillus strains towards phytopathogenic fungi* by RAMÍREZ-MARTÍNEZ, Javier & PACHECO-AGUILAR, Juan Ramiro, with adscription in the Universidad Autónoma de Querétaro.

Content

Article **Journal Simulation and Laboratory**
December 2022 Vol.9 No.27 1-13

Comparison of Vegsyst and Hortsyt models: Two models of growth of greenhouse crops

Comparación de los modelos Vegsyst y Hortsyt: Dos modelos de crecimiento de cultivos en invernadero

MARTINEZ-RUIZ, Antonio*†, QUINTANAR-OLGUIN, Juan, SERVÍN-PALESTINA, Miguel and FLORES-DE LA ROSA, Felipe Roberto

Instituto Nacional de Investigaciones Forestales Agrícolas y Pecuarias (INIFAP), México.

ID 1st Author: *Antonio, Martinez-Ruiz* / **ORC ID**: 0000-0001-6555-4651, **CVU CONACYT ID**: 364739

ID 1st Co-author: *Juan, Quintanar-Olguin* / **ORC ID:** 0000-0003-2388-5027, **CVU CONACYT ID**: 203741

ID 2nd Co-author: *Miguel Servín-Palestina* / **ORC ID:** 0000-0003-4070-1234, **CVU CONACYT ID**: 296877

ID 3rd Co-author: *Felipe Roberto Flores-de la Rosa* / **ORC ID:** 0000-0002-1435-936X, **CVU CONACYT ID**: 535996

DOI: 10.35429/JSL.2022.27.9.1.13 Received June 30 2022; Accepted December 30, 2022

Abstract

The HortSyst model is a new discrete-time model to describe the dynamics of photothermal time (PTT), dry matter production (DMP), N uptake (Nup), leaf area index (LAI) and rate of transpiration (ETc) of greenhouse crops, it has 13 parameters. The model assumes that crops do not have water and nutrient limitations. The input variables of the model are hourly measurements of air temperature, relative humidity, and the integral of solar radiation. Two experiments were carried out in a greenhouse, with hydroponic tomato cv. "CID F1" at a density of 3.5 plants m^{-2}, autumn-winter and spring-summer cycle, in Chapingo, Mexico. The first experiment was transplanted on August 21, 2015 and the second experiment on April 24, 2016. A weather station was installed inside the greenhouses, temperature and relative humidity were measured with a model S-TMB-M006 sensor and radiation global sensor S-LIB-M003. The objective of this research is to compare two growth models for tomato in greenhouses. According to the adjustment of its predictions against the measurements it can be of help in the supply water and nitrogen.

Wáter consumption, Water use efficiency, Nutritional extraction

Resumen

El modelo HortSyst es un nuevo modelo de tiempo discreto para describir la dinámica del tiempo fototérmico (PTT), la producción de materia seca (DMP), la absorción de N (Nup), el índice de área foliar (LAI) y la tasa de transpiración (ETc) de cultivos de invernadero, cuenta con 13 parámetros. El modelo asume que los cultivos no tienen limitaciones de agua y nutrientes. Las variables de entrada del modelo son mediciones horarias de la temperatura del aire, la humedad relativa y la integral de la radiación solar. Se realizaron dos experimentos en invernadero, con jitomate hidropónico *cv*. "CID F1" a una densidad de 3.5 plantas m^{-2}, de ciclo otoño-invierno y primavera-verano, en Chapingo, México. El primer experimento se trasplantó el 21 de agosto de 2015 y el segundo experimento el 24 de abril de 2016. Se instaló una estación meteorológica dentro de los invernaderos, se midió temperatura y humedad relativa con un sensor modelo S-TMB-M006 y la radiación global sensor S-LIB-M003. El objetivo de esta investigación es comparar dos modelos de crecimiento para jitomate en invernadero. De acuerdo con el ajuste de sus predicciones frente a las mediciones puede ser de ayuda en el suministro de agua y N.

Consumo hídrico, Eficiencia del uso del agua, Extracción nutrimental

Citation: MARTINEZ-RUIZ, Antonio, QUINTANAR-OLGUIN, Juan, SERVÍN-PALESTINA, Miguel and FLORES-DE LA ROSA, Felipe Roberto. Comparison of Vegsyst and Hortsyt models: Two models of growth of greenhouse crops. Journal Simulation and Laboratory. 2022, 9-27: 1-13

*Correspondence to Author (e-mail: amartinezr8393@gmail.com.mx)
†Researcher contributing as first Author.

Introduction

Plant growth modelling has become a key research activity, particularly in the fields of agriculture, forestry and environmental sciences. Due to the growth of computer power and resources and the sharing of experiences between biologists, mathematicians and computer scientists, the development of plant growth models has progressed enormously during the last two decades. The use of an interdisciplinary approach is necessary to advance research in plant growth modelling and simulation (Thornley and France, 2007; Fourcaud *et al.,* 2008).

The efficient management of intensive agriculture demands consideration of the factors that determine the crop production potential and their interactions. The integration of these factors under the systems approach and based on growth simulation models is an approximation that allows the design of practices of management aimed at increasing productivity by minimizing the environmental impact caused by agricultural activity (Stockle *et al.,* 1994).

To increase knowledge of cropping systems and to look for practical applications, several models have been developed for greenhouse crops. Specifically for tomatoes have been proposed TOMGRO (Jones *et al*., 1991), TOMSIM (Heuvelink *et al*., 1999), TOMPOUSSE (Abreu *et al*., 2000) models, which have helped to simulate the behavior of production systems. However, some of these models are too complex because they involve too many state variables, input variables or model parameters, which make their implementation difficult. For example the model TOMGRO ver. 1.0 has 69 state variables, TOMGRO ver. 3.0 has 574 state variables, or the simplified version of this same model that presents 5 state variables and 29 parameters (Vazquez *et al*., 2014). Other models for greenhouse crops, although simpler, have been developed for crop systems specific to a region such as the VegSyst model (Gallardo *et al*., 2011; Gimenez *et al*., 2013; Gallardo *et al*., 2014; Gallardo *et al*., 2016).

In order to have an optimal control in the management of productive systems, it is necessary to develop models with the capacity to represent the interactions that exist between the development of the crop, climatic conditions and physiological processes of water and nutrients uptake. Thus, to find the concentration of the optimal nutrient solution, is the most desirable in a production system, this fact considers an important effect of the transpiration and irrigation management on the nutritional absorption since the dissolved ions in the nutrient solution are transported from the root through mass flow, in which transpiration is the process that provides the necessary force for the movement to occur (Mengel *et al*., 2001).

Therefore, with the use of a mathematical model, the perfect synchronization between the amounts of water required for growth and the nutritional demand of the crop depending on the environmental conditions, allows efficient use of water in the greenhouse crops. Nowadays, some of the scheduling of irrigation of hydroponic culture mode used in greenhouses is based either on time clock or by radiation method, but some of these are not flexible enough to satisfy the varying crop water requirements through the day and during de season, in case of time clock, and another as, the radiation method does not take into account the influence of vapor pressure deficit so this method is an approach of the reality, but not the complete solution according to (Lizarraga *et al*., 2003).

The HortSyst model is a new discrete time dynamic model that predicts: photo-thermal time, dry matter production, N uptake, leaf area index and crop transpiration rates. The development of this model started by modifying the structure of the VegSyst model (Gallardo *et al*., 2011; Gimenez *et al*., 2013; Gallardo *et al*., 2016) proposed for greenhouse crops. However, these modifications became increasingly large and ended up being a new model considerably simpler and with predictive quality equal or greater than the VegSyst model. The objective of this work is to describe the mathematical model HortSyst that was developed as a tool capable of being used by producers in the decision making on the nitrogen supply from the simulation of biomass production and irrigation programming using the transpiration in a crop of hydroponic tomato (*Solanum lycopersicom* L.) in greenhouse

ISSN: 2410-3462

Materials and methods

HortSyst Model Description

The HortSyst model is a nonlinear dynamic growth model for hydroponic systems, for tomato (*Solanum lycopersicom* L.) in greenhouses. This model was developed to be used as a tool for decision support systems in Mexican greenhouses. The model assumes that crops have no water and nutrient limitations, also that the crop is free of pests and diseases, and under management in cultural activities like commercial greenhouses.

The HortSyst model predicts crop biomass production ($DMP, g\ m^{-2}$), N uptake ($Nup, g\ m^{-2}$), photo-thermal time ($PTI, MJ\ d^{-1}$) as state variables and the crop transpiration rates (ETc, kgm^{-2}) and leaf area index ($LAI\ , m^2m^{-2}$) as output variables. The model inputs variables are hourly measurements of air temperature (°C), relative humidity (%), and integral of solar radiation (Wm^{-2}). It has thirteen parameters (Table 1) besides initial conditions of dry matter production and photo-thermal time. The HortSyst model was developed based on the VegSyst model (Gallardo *et al*., 2011; Gallardo *et al*., 2016; Gallardo *et al*., 2014; Giménez *et al*., 2013; Granados *et al*., 2013; Gallardo *et al*., 2016).

The following Forrester diagram (Figure 1) summarizes the functional relationship that exists between the components of the model as input, output, parameters and state variables.

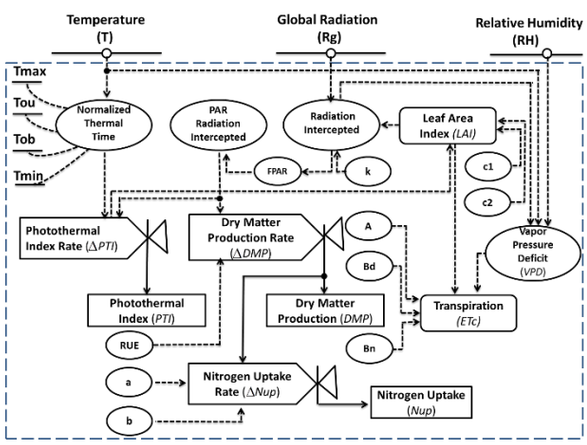

Figure 1 Forrester diagram for HortSyst model

The HortSyst model predicts in discrete time, namely, by means of difference equations the behavior of the three state variables: the photo-thermal time (eq.1), the dry matter production (eq.2) and the nitrogen uptake (eq.3).

$$PTI(j+1) = PTI(j) + \Delta PTI \quad (1)$$

$$DMP(j+1) = DMP(j) + \Delta DMP \quad (2)$$

$$N_{up}(j+1) = N_{up}(j) + \Delta N_{up} \quad (3)$$

where the values of each variable in discrete time $j+1$ are calculated by adding the values of the variables in the previous discrete time j plus the rate of change Δ corresponding to each variable.The variable photo-thermal time ($PTI, MJ\ d^{-1}$) is defined as the state variable since it couples the effect of radiation and temperature on the crop and from the point of view of the climate of the greenhouse, these variables are not strongly correlated as they are in the open field (Reffye *et al*., 2009; Xu *et al*., 2010). In contrast to other researchers who have modeled the leaf area index as a function of time or as a function of the day degrees (Carmassi *et al*., 2013; Chin *et al*, 2011; Incrocci *et al*., 2008; Massa *et al*., 2011; Medrano., 2008; Montero., 2001; Orgaz *et al*., 2005) or others who have used the days after transplant (Carmassi *et al*., 2007; Medrano., 2005; Medrano *et al*., 2011; Ta *et al*., 2011) or the specific leaf área (Bechini *et al*, 2006; Stockle *et al*, 2003), in the HortSyst model, the photo-thermal time state variable as the independent variable of the leaf area of the crop. In the VegSyst model, the thermal time is the state variable that drives the daily calculation of biomass production, nitrogen uptake and crop evapotranspiration (Gallardo *et al*., 2011; Gimenez *et al*., 2013). In addition, radiation directly influences crop growth (dry matter production) and affects development (morphogenesis) (Sergio *et al*., 2003).

The rate of change of the photo-thermal time (ΔPTI) depends on the photosynthetically active radiation(PAR), normalized thermal time (TT) and the intercepted fraction of radiation(f_{i-PAR}).

$$\Delta PTI(j) = \left(\sum_{i=1}^{24} TT(i,j)\right) / 24 \times PAR(j) \times f_{i-PAR}(j) \quad (4)$$

ISSN: 2410-3462

where the index i represents hourly calculations, index j represents daily level, PAR is photosynthetically active radiation and is calculated from daily global radiation above the crop (R_g,$W\ m^{-2}$).

$$PAR = 0.5 \times R_g \quad (5)$$

TT °C is the normalized thermal time as used by other researchers (Bechini *et al*., 2006; Soltani *et al*., 2012), which is defined as the ratio of the rate of growth under real conditions of optimal temperatures, and is calculated as follows:

$$T = \begin{cases} 0 & (T_a < T_{min}) \\ (T_a - T_{min})/(T_{ob} - T_{min}) & (T_{min} \le T_a < T_{ob}) \\ 1 & (T_{ob} \le T_a \le T_{ou}) \\ (T_{max} - T_a)/(T_{max} - T_{ou}) & (T_{ou} < T_a \le T_{max}) \\ 0 & (T_a > T_{max}) \end{cases} \quad (6)$$

where T_a (°C) is the temperature of the air, T_{min} (°C) is the minimum temperature, T_{max} (°C) is the maximum temperature, T_{ob} (°C) is the lower optimal temperature and T_{ou} (°C) is the upper optimal temperature. The intercepted fraction of the radiation is calculated by the exponential function:

$$f_{i-PAR} = 1 - exp(-k \times LAI(j)) \quad (7)$$

where k is the light extinction coefficient, and LAI is the leaf area index which in turn is calculated from the leaf area value A_f (m^2) which depends on the daily photo-thermal time (ΔTPI) by an equation type Michaellis-Menten

$$LAI(j) = \left(\frac{c_1 PTI(j)}{c_2 + PTI(j)}\right) d \quad (8)$$

where c_1 (m^{-2}) and c_2 are parameters of the Michaellis-Menten equation and d (plants m^{-2}) is the density of the crop.

The model uses a classical concept approach, efficient radiation applications (Kang *et al*., 2008; Lemaire *et al*., 2008; Reffye *et al*., 2009) which allows the calculation of daily dry matter production (ΔDMP) as a function of the photosynthetically active radiation (PAR) eq. (5), crop characteristics such as leaf area index (LAI) eq. (8) and the radiation use efficiency parameter (RUE, gMJ^{-1}) as has proposed by several researchers (Gallardo *et al*., 2016; Shibu *et al*., 2010; Soltani and Sinclair, 2012).

$$\Delta DMP(j) = RUE \times f_{i-PAR} \times PAR(j) \quad (9)$$

The value of (ΔDMP) accumulates day by day as in equation (2) Once the daily dry matter production is calculated, it is possible to calculate the nitrogen uptake daily by the equation(10, 11) (Le Bot *et al*., 1998; Tei *et al*., 2002) which, when accumulated with equation (3), allows the calculation of the nitrogen extraction throughout the crop growing period (ΔDMP).

$$\%N(j) = a \times (DMP(j))^{-b} \quad (10)$$

$$N_{up}(j) = (\%N(j)/100) \times DMP(j) \quad (11)$$

where ΔN_{up} is the daily uptake nitrogen ($g\ m^{-2}$), a and b are parameters of the equation and ΔDMP is the increase of daily dry matter produced ($g\ m^{-2}$).

Finally, crop transpiration ($ETc, kg\ m^{-2}$) is calculated every hour using the equation proposed by (Baille *et al*., 1994), which has been widely used to schedule greenhouse irrigation (Carmassi *et al*., 2013; Martínez-Ruiz *et al*., 2012; Massa *et al*., 2011; Medrano *et al*., 2011). The Baille transpiration model requires the global radiation data, vapor pressure deficit, which is calculated with values of air temperature and relative humidity and leaf area index equation (8). The equations that in HortSyst estimate the transpiration of the crop are:

$$ETc(i) = A \times (1 - \exp(-k \times LAI(j))) \times Rg(i) + LAI(j) VPD(i) B_{(d,n)} \quad (12)$$

$$ETc(j+1) = \sum_{i=1}^{24} ETc(i) \quad (13)$$

where $ETc(j+1)$ ($kg m^{-2} d^{-1}$) is the daily accumulated transpiration, $ETc(i)$ ($g\ m^{-2} h^{-1}$) is the hourly transpiration rate, R_g is the hourly incident solar radiation ($W\ m^{-2}$), VPD is the vapor pressure deficit and A (dimensionless) refers to the radiative parameter; and B_d, B_n ($W m^2 kPa^{-1}$) are parameters of the aerodynamic term of equation (28) for day and night, respectively. All the parameters of HortSyst are described in Table 1.

ISSN: 2410-3462

The computational model

The HortSyst is currently programmed in the Matlab computer environment. The dynamic equations are coded inside a Matlab subroutine (function). Two iterative loops allow computing daily and hourly calculations. The outputs of the subroutine are the variables; photo-thermal time, crop biomass, nitrogen uptake, crop evapotranspiration and leaf area index. The input variables of the subroutine are the model parameters (Table 1) and climatic variables. A main program (Matlab script) calls the subroutine and generating graphs or other calculations necessary to run the simulations.

Tomato growth experiments description

Two experiments were carried out under greenhouse conditions, during the autumn-winter, and spring-summer season, located at the University of Chapingo, Mexico. Geographical location: 19° 29' LN, 98° 53' and 2240 msnm. A tomato (*Solanum lycopersicom* L.) crop cultivar "CID F1" was grown in a hydroponic system using volcanic sand as substrate and fertilized with Steiner nutrient solution (Steiner, 1980). Plants were distributed with a density of 3.5 plants m^{-2}. For the first experiment tomato seeds were sown on 18 July 2015 and the plants were transplanted on 21 August 2015 in a glass greenhouse type chapel with 8 x 8 m dimension, and the second experiment were sown on 24 March 2016 and transplanted on 24 April 2016 in a plastic greenhouse with overhead ventilation with dimension of 8 x 15 m.

A weather station (Onset Computer Corporation) was installed inside of the greenhouses. Temperature and relative humidity were measured with a S-TMB-M006 model sensor placed at a height of 1.5 m. Global radiation was measured with a S-LIB-M003 sensor and was located 3.5 m above the ground.

Both sensors were connected to a datalogger U-30-NRC model, which recorded data every minute. In each experiment, three plants were chosen randomly for the sample each 10 days to measure dry matter, nitrogen uptake accumulation and leaf area index. Plants were dried out during 72 h at 70 °C. And nitrogen was determined by Micro-Kjeldahl method (Chapman and Pratt, 1974).

Leaf area Index were determinate by a nondestructive method, it consisted in taking 4 plants randomly to get measurements of width and length of the plants leaves and also the total leaf area and a plant canopy analyzer LAI-3100 (LICOR, USA) was used. From the measurements, nonlinear regressions models were fitted in order to estimate this variable. The crop transpiration rate was measured every minute by means of a weighing lysimeter located in a central row of the greenhouses, the device includes an electronic balance (scale capacity =120 kg, resolution ± 5 g equipped with a tray carrying 4 plants for both experiments. The weight loss measured by the electronic balance was assumed equal to the crop transpiration. To compare the predictive quality of the HortSyst and VegSyst models we used the nominal parameters listed in Table 1 for the HortSyst model and the parameters used for the simulation VegSyst model were taken from (Gallardo *et al*.,2014, Gallardo *et al*., 2016). And MAE and RMSE statistics were considered to evaluate the performance of simulation of both models.

No	Parameter	Symbol	Units	Nominal Value (autumn-winter)	Nominal Value (spring-summer)	source
1	Top upper temperature	T_{max}	°C	35.00	35.00	Peet and Welles (2005), Chu *et al*., (2009)
2	Top bottom temperature	T_{min}	°C	10.00	10.00	Peet and Welles (2005), Chu et al., (2009)
3	Optimum minimum temperature	T_{ob}	°C	17.00	17.00	Peet and Welles (2005)
4	Optimum maximum temperature	T_{ou}	°C	24.00	24.00	Peet and Welles (2005)
5	Radiation Use Efficiency	RUE	g MJ^{-1}	4.01	3.1	Gallardo *et al*., (2014), Challa and Bakker (1998)
6	Extinction coefficient	k	---	0.70	0.70	
7	N concentration in the dry biomass at the end of the exponential growth period	a	g m^{-2}	0.755	7.55	Gallardo *et al*., (2014)
8	Is the slope of the relationship	b	---	-0.15	-0.15	Gallardo *et al*., (2014)
9	Slope of the curve	c_1	m^{-2}	2.82	3.07	Estimated
10	Intersection coefficient	c_2	---	74.66	175.64	Estimated
11	Radiative coefficient	A	---	0.59	0.24	Montero *et al*., (2001), (Medrano *et al*., (2008)
12	Aerodynamic coefficient during day	B_d	$Wm^{-2}kPa^{-1}$	19.10	37.6	Montero *et al*., (2001),Medrano *et al*., (2008)
13	Aerodynamic coefficient during night	B_n	$Wm^{-2}kPa^{-1}$	25.00	26	Montero *et al*.,(2001), Medrano *et al*.,(2008)

Table 1 Model parameters used for HortSyst model during greenhouse growing condition.

Results

Simulation of HortSyst Model: Input variables

The global solar radiation (Rg), air temperature (Ta), and relative humidity (RH) used in the simulations of the HortSyst and VegSyst model for both growing periods autumn- Winter (O-W) and spring summer (S-S) crop cycle are showed in Figure 2, 3 and 4, respectively.

ISSN: 2410-3462

The nominal values of the model parameters are given in Table 1. According to measured data it is clear that the amount of global radiation in the spring summer season is a more than twice the one is reached in the autumn-winter season. Furthermore, during autumn-winter we observed greater cloudy days. This fact has its effect on the accumulation of dry matter, nitrogen uptake, leaf area index and water uptake (transpiration).

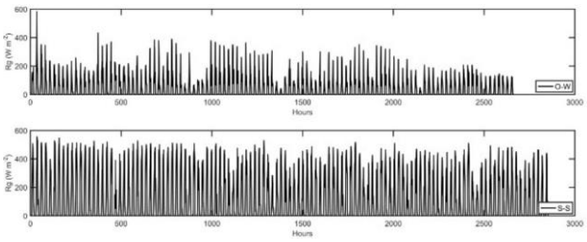

Figure 2 Global radiation measured hourly inside of the greenhouse located in Chapingo, Mexico during outum-winter (O-W), 2015, and Spring-Summer (S-S), 2016

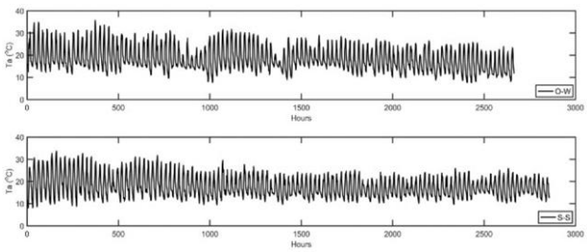

Figure 3 Air temperature measured hourly inside of the greenhouse, located in Chapingo, Mexico, during outum-winter (O-W), 2015 and Spring-Summer (S-S), 2016

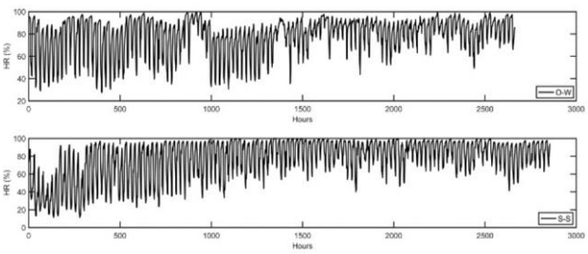

Figure 4 Relative Humidity measured hourly inside of the greenhouse located in Chapingo, Mexico, during outum-winter (O-W), 2015 and Spring-Summer (S-S), 2016

Dry matter Production (DMP)

Figure 5 shows the values of the simulation for dry matter production using RUE values of 4.01 g MJ^{-1} for the autumn-winter and RUE of 3.01 g MJ^{-1} for the spring summer, where it is observed that during the spring summer season for both HortSyst and VegSyst models, there was approximately twice the biomass with respect to the autumn-winter, this is due to the fact that it is the cycle in which there is more solar radiation (Figure 2).

It was found that the simulation follows the trend of the measured values in laboratory having as accumulated final value of simulated biomass in the autumn-winter cycle of 587.37 g m^{-2} against a measured value of 673.38 g m^{-2} which represents an underestimation of the model of 12.77% of the measured value. In case of the spring-summer period, the simulated value at the end of the cycle is 1336.59 g m^{-2} against the measured 1304.118 g m^{-2}, resulting in an overestimation error of 2.49%. This means that the RUE value considered could be used for the simulation of the biomass.

In both experiments total dry matter production shows an exponential growth and then an approximately linear growth phase, which is a growth pattern, expected under constant climate conditions.

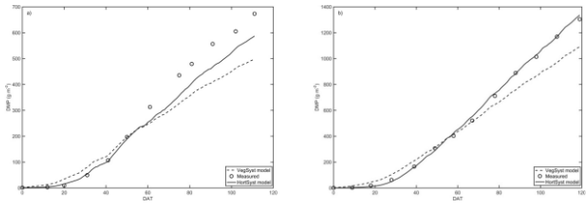

Figure 5 Time course of the simulated and measured values of dry matter production of a greenhouse tomato crop grown in Chapingo, Mexico, for a) autumn-winter, 2015 and b) spring-summer, 2016 for HortSyst and VegSyst models

Nitrogen Uptake (Nup)

On the other hand, Figure 6 shows a comparison between the values measured and predicted by the HortSyst model and VegSyst model, for the nitrogen uptake variable for both crop seasons.

In both cases a good fit between simulations and measurements is observed for the case of nitrogen uptake in autumn-winter, the final value predicted by the simulation is 19.98 g m^{-2} against the measured value of 13.71 g m^{-2} which represents an error of 45.78%. In case of Spring-Summer the value simulated was 40.23 g m^{-2} and the measured was 27.4 g m^{-2}. In both periods error of predicted value by the model is approximately of 46% above measurements (Figure 6).

ISSN: 2410-3462

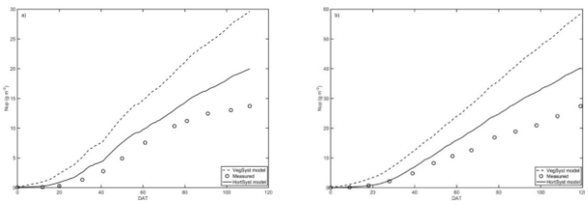

Figure 6 Time course of the simulated and measured values of Nitrogen uptake of a greenhouse tomatocrop grown in Chapingo, Mexico, for a) autumn-winter, 2015 and b) Spring-Summer, 2016, for HortSyst and VegSyst models

Leaf Area Index

Because the lack of information in the literature of the parameters values of this variable (c_1 and c_2) a manual calibration was carried out in order to determine the possible values could be used in the simulation for each growing period. It is possible that, this variable plays central role in the model since, from these simulated values is predicted photo-thermal time, dry matter production, transpiration and indirectly nitrogen uptake. The considered values for the parameters are showed in Table 1. Their values are longer for spring-summer than for autumn-winter.

The simulated LAI values are similar to the measured values 5.85 m^2m^{-2} with an error of 0.4% between the measured and simulated data (5.83 m^2m^{-2}), during autumn-winter and during spring-summer, the measured LAI was 7 m^2m^{-2}, against 6.86 m^2m^{-2} with an error of 2.17% for the measured and simulated data as shown in the figure 7.

LAI is only simulated by the HortSyst model. The VegSyst model does not take in account the computation of LAI, because it uses another concept like heat units and intercepted PAR radiation for two stages of the crop.

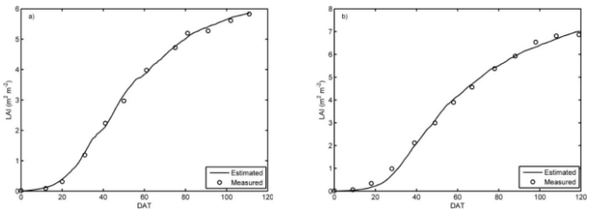

Figure 7 Time course of the simulated and measured values of the Lea Area Index of a greenhouse tomato crop grown in Chapingo, Mexico for, a) Autumn-Winter, 2015 and b) Spring-Summer, 2016, for HortSyst model.

Crop transpiration rate

For the transpiration variable (Figure 8), it was found that using the parameters values shown in Table 1 for A, Bd and Bn, it is acceptable to estimate with an error of 2. 62%, for an accumulated simulated value of 183.68 kg m-2 and measured values and 188.49 kg m-2 at the end of the cycle autumn-winter and measured value of 291.69 kg m-2 against simulated of 294.2 kg m-2 with error of 0.88% for spring and summer, respectively.

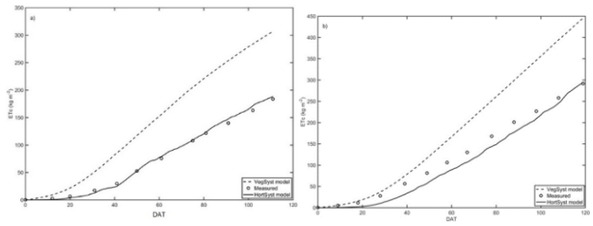

Figure 8 Time course of the simulated and measured values of crop transpiration of a greenhouse tomato crop grown in Chapingo, Mexico a) Autumn-Winter, 2015 and b) Spring-Summer, 2016, for HortSyst and VegSyst models

Photo-thermal time

Figure 9 shows the photo-thermal time variable that uses this model to calculate the leaf area index which presents a behavior similar to that previously reported by Xu *et al.,* (2010). It is important to emphasize that this simulation is intended to demonstrate the ability of the model to predict the most important variables related to the production of a hydroponic tomato crop under greenhouse conditions and using volcanic sand ("tezontle") as substrate. Using the temperature at 1.5 m above ground and PAR above canopy this photo-thermal model eq. (4) gave satisfactory prediction of leaf area index eq.(8)

The amount of photo-thermal time accumulated in autumn winter was 108.97$MJ\ d^{-1}$ and for spring summer of 327.56 $MJ\ d^{-1}$ representing a 3 times greater difference in spring- summer. Like LAI variable the HortSyst model simulates PTI during the crop cycle this is the main difference between HortSyst and VegSyst model.

ISSN: 2410-3462

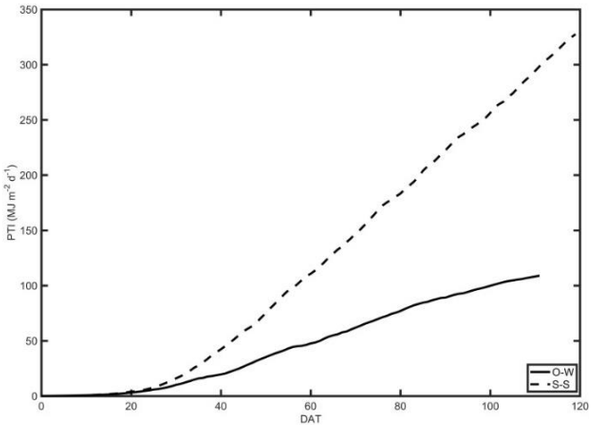

Figure 9 Time course of the predicted of photo-thermal time by HortSyst model, accumulated since plant date for Autumn-Winter (O-W) and Spring-Summer (S-S)

From the simulations carried out for the HortSyst and VegSyst model, the HortSyst model provides better predictive quality for dry matter production, nitrogen uptake and transpiration than the VegSyst model, this is confirmed by the higher values of the statistics; MAE and RMSE (Table 2) for this last model for both crop season, spring-summer and autumn-winter, with the highest errors for the case of transpiration in the VegSyst model. The variable leaf area index was not compared since both models do not share the simulation of this variable in its mathematical structure.

	HortSyst Model		**VegSyst Model**	
	Autumn-Winter			
OUTPUT	MAE	RMSE	MAE	RMSE
DMP	39.35	53.60	69.70	93.04
Nup	2.56	3.19	7.29	8.82
ETc	3.51	4.37	67.77	80.49
LAI	0.09	0.10		
	Spring-Summer			
DMP	12.93	16.71	70.14	101.17
Nup	5.25	7.03	13.54	16.99
ETc	15.94	18.16	59.96	79.53
LAI	0.12	0.14		

Table 2 Summary of results of the statistical indices (MAE and RMSE) used to evaluate the performance of the HortSyst model and VegSyst model for simulation of DMP, Nup, ETc and LAI during Autumn-Winter, 2015 and Spring-Summer, 2016

In order to show a potential use of the HortSyst model to predict the concentration of nitrogen uptake by the crop as a function of the transpiration, in figure 10 shows daily N absorbed concentration, considering the amount of water absorbed daily by the process of transpiration predicted by the model, for the spring-summer and autumn-winter crop cycles.

Where in the first 35 days, the uptake concentration by crop exceeds the concentration of 12 me L^{-1} (168 mgL^{-1}) recommended by Steiner (1980), after 40 days of cultivation, the concentration decreases approximately half of the concentration applied to the crop. With the evaluation of performance of the model, it was found that it would be a waste of approximately 50% of the applied fertilizer considering an efficiency of 100% of the system production under soilless culture.

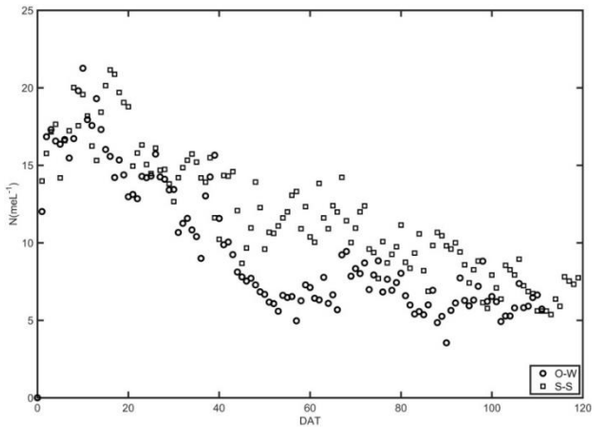

Figure 10 Time course of simulation of daily value of N concentration (meL-1) nitrogen uptake during Autumn-Winter (O-W), 2015 and Spring-Summer (S-S), 2016

Discussion

The crop simulation models HortSyst and VegSyst were simulated to show its performance for tomato for Mexican greenhouses. HortSyst model predicts correctly crop biomass, photo-thermal time and predicts accurately leaf area index and transpiration crop, however the quality of prediction of N uptake is poor using the nominal parameter values. This means that to improve the predictive quality of the model not only for N uptake but also for the other variables parameter estimation of model calibration is required by using experimental data. The quality of the simulated values of dry matter production are acceptable, because of the results obtained in the simulation using the RUE value of 4.01 g MJ^{-1} for prediction of biomass reported by (Gallardo *et al*., 2016) and RUE 3.01 g MJ^{-1} reported by (Challa and Bakker, 1998), for tomato crop, biomass values at the end of cycle are slightly lower than those reported by Gallardo *et al*., (2014) for autumn-winter. The value of this parameters are different due to differences in climatic conditions between one region and another or to different crop cycles (Villegas - Cota *et al*., 2014).

ISSN: 2410-3462

The measured N uptake values were quite similar to those results reported for tomato crop by Gallardo *et al*., (2016); Gallardo *et al*. (2014). The differences in the values accumulated for nitrogen uptake between both cycles at the end of these are because in each cycle the environmental conditions are not the same at least in the levels of radiation and maybe the temperature variation between the day and night. The parameters used in the model for these variables were the same for the two crop cycles reported by Gallardo *et al*. (2016); Gallardo *et al*. (2014) since no values were found for each different cultivation period, in both cases the model did not show a satisfactory fit because the authors calibrated the model for nitrogen in a different culture system.

The modeling of LAI is one of the important differences with respect to the VegSyst model proposed by (Gallardo *et al*., 2011, 2016, 2014; Giménez *et al*., 2013; Granados *et al*., 2013), since these authors did not include the simulation of this variable in their model.

The final accumulated measured of evapotranspiration value for the autumn- winter is similar to those reported by (Gallardo *et al*., 2016; Gallardo *et al*., 2014). It is important to mention that the methodology to model water consumption by these authors was different since they used the Penman-Monteith model with crop coefficients. The values of the parameters in the HortSyst model are slightly similar to those reported by (Martínez-Ruiz *et al*., 2012) since these authors performed the calibration using frequent climatic data of 15 minutes and hourly.

In case of photo-thermal time Xu *et al*. (2010) found that modeling the leaf area index using this concept gave better predictions than degrees days model as (Gallardo *et al*., 2016) the latter type of models overestimate the predictions because of the fact that inside of the greenhouse the global radiation is not synchronized with the temperature behavior (De Reffye *et al*., 2003; Xu *et al*., 2010).

On the other hand, when comparing the estimation of leaf area index using the specific leaf area as used in Stockle *et al*. (1994) presents a poorest predictions due to the large variation of the specific leaf area among different growing seasons and the data of this latter variable can only be obtained by destructive measurements, this limits the application of models based on specific leaf area to greenhouse crops and climate management practice (Xu *et al*., 2010).

The advantage of using a model to make fertilization recommendations is that it considers factors as; environment conditions, physiological processes such as transpiration and characteristics of the crop as leaf area index and biomass production. The results found that with the model without calibration the simulation are quite similar to those reported (Gallardo *et al*., 2014) for the Autumn-winter season, who evaluated the use of the model VegSyst under three scenarios of recommendation of fertilization.

Conclusions

The HortSyst model can be used as a decision-making tool in greenhouse production systems, since according to the presented simulation it predicts in an acceptable way the biomass, absorbed nitrogen, leaf area index and transpiration. To model the leaf area index, a new concept called the photo-thermal time, which represents the effect of temperature on leaf expansion and the effect of radiation on crop growth, which, may be used as an alternative to simulate leaf area index in crop models. In fact, there are few models that include the variable transpiration in order to be used in irrigation management, in this case, was used a model that was derived from the simplification of Penman-Monteith and for its simplicity can be used to predict the consumption of water by the crop, in addition it needs climatic variables that are commonly measured in greenhouses.

It is necessary to carry out a calibration of the model to find the values of the parameters that help to improve its predictive quality. Also is necessary carrying out an evaluation (validation) of the model, with data of another experiment of the same cycle or different crop cycle to evaluate its behavior under different scenarios.

ISSN: 2410-3462

Due to the small number of parameters (13 parameters) involved in the HortSyst model it is feasible to use it for irrigation management and nitrogen application in hydroponic tomato under greenhouse.

References

Abreu, P., Meneses, J. F., & Gary, C. (2000). Tompousse, a model of yield prediction for tomato crops: Calibration study for unheated plastic greenhouses. *Acta Horticulturae,* 519, 141–149. 10.17660/ActaHortic.2000.519.14

Baille, M., Baille, A., & Laury, J. C. (1994). A simplified model for predicting evapotranspiration rate of nine ornamental species vs. climate factors and leaf area. *Scientia Horticulturae*, *59*(3–4), 217–232. https://doi.org/10.1016/0304-4238(94)90015-9

Bechini, L., Bocchi, S., Maggiore, T., & Confalonieri, R. (2006). Parameterization of a crop growth and development simulation model at sub-model components level. An example for winter wheat (Triticum aestivum L.). *Environmental Modelling & Software*, *21*, 1042–1054. https://doi.org/10.1016/j.envsoft.2005.05.006

Carmassi, G., Bacci, L., Bronzini, M., Incrocci, L., Maggini, R., Bellocchi, G., … Pardossi, A. (2013). Modelling transpiration of greenhouse gerbera (Gerbera jamesonii H. Bolus) grown in substrate with saline water in a Mediterranean climate. *Scientia Horticulturae*, *156*, 9–18. https://doi.org/10.1016/j.scienta.2013.03.023

Carmassi, G., Incrocci, L., Maggini, R., Malorgio, F., Tognoni, F., & Pardossi, A. (2007). An aggregated model for water requirements of greenhouse tomato grown in closed rockwool culture with saline water. *Agricultural Water Management*, *88*(1–3), 73–82. https://doi.org/10.1016/j.agwat.2006.10.002

Challa, H., Bakker, J. (1998). Potential production within the greenhouse environment . In:ENOCH, Z.;STANHILL, G., (Eds) Ecosystems of the world. The greenhouse ecosystem. Amsterdam: Elsevier, p. 133-348.

Chapman, H. D. & Pratt P.E. (1974).Methods of analysis for soil, plants and waters. Davis, Calif. Univ. of California, Div. of Agricultural Science.

Chin, D. A., Fan, X. H., & Li, Y. C. (2011). Validation of Growth and Nutrient Uptake Models for Tomato on a Gravelly South Florida Soil Under Greenhouse Conditions. *Pedosphere*, *21*(1), 46–55. https://doi.org/10.1016/S1002-0160(10)60078-1

Chu, J.-X., Sun, Z.-F., Du, K.-M., Jia, Q., & Liu, S. (2009). Establishment of Dynamic Model for the Nutrient Uptake and Development about Tomato in Greenhouse. In W. Cao, J. W. White, & E. Wang (Eds.), Crop Modeling and Decision Support (pp. 54–58). Berlin, Heidelberg: Springer Berlin Heidelberg. https://doi.org/10.1007/978-3-642-01132-0_6

Villegas-Cota, J. R., González-Hernández, V. A., Carrillo-Salazar, J. A., Livera-Muñoz, M., Sánchez-del Castillo, F., & Osuna-Enciso, T. (2004). Crecimiento y rendimiento de tomate en respuesta a densidades de población en dos sistemas de producción. Revista Fitotecnia Mexicana, 27(4), 333-333.

De Reffye, P., & Hu, B. G. (2003). Relevant Qualitative and Quantitative Choices for Building an Efficient Dynamic Plant Growth Model: GreenLab Case. *International Symposium on Plant Growth Modeling, Simulation, Visualisation and Their Applications*, 87–106.

Fourcaud, T., Zhang, X., Stokes, A., Lambers, H., & Körner, C. (2008). Plant growth modelling and applications: The increasing importance of plant architecture in growth models. *Annals of Botany*. https://doi.org/10.1093/aob/mcn050

Gallardo, M., Fernandez, M. D., Gimenez, C., Padilla, F. M., & Thompson, R. B. (2016). Revised VegSyst model to calculate dry matter production, critical N uptake and ETc of several vegetable species grown in Mediterranean greenhouses. *Agricultural Systems*, *146*, 30–43. https://doi.org/10.1016/j.agsy.2016.03.014

Gallardo, M., Gimenez, C., Martínez-Gaitán, C., Stöckle, C. O., Thompson, R. B., & Granados, M. R. (2011). Evaluation of the VegSyst model with muskmelon to simulate crop growth, nitrogen uptake and evapotranspiration. *Agricultural Water Management*, *101*(1), 107–117. https://doi.org/10.1016/j.agwat.2011.09.008

ISSN: 2410-3462

Gallardo, M., Thompson, R. B., Gimenez, C., Padilla, F. M., & Stöckle, C. O. (2014). Prototype decision support system based on the VegSyst simulation model to calculate crop N and water requirements for tomato under plastic cover. *Irrigation Science*, *32*(3), 237–253. https://doi.org/10.1007/s00271-014-0427-3

Gimenez, C., Gallardo, M., Martínez-Gaitán, C., Stöckle, C. O., Thompson, R. B., & Granados, M. R. (2013). VegSyst, a simulation model of daily crop growth, nitrogen uptake and evapotranspiration for pepper crops for use in an on-farm decision support system. *Irrigation Science*, *31*(3), 465–477. https://doi.org/10.1007/s00271-011-0312-2

Granados, M. R., Thompson, R. B., Fernández, M. D., Martínez-Gaitán, C., & Gallardo, M. (2013). Prescriptive-corrective nitrogen and irrigation management of fertigated and drip-irrigated vegetable crops using modeling and monitoring approaches. *Agricultural Water Management*, *119*, 121–134. https://doi.org/10.1016/j.agwat.2012.12.014

Heuvelink, E. (1999). Evaluation of a Dynamic Simulation Model for Tomato Crop Growth and Development. *Annals of Botany*, *83*, 413–422. https://doi.org/10.1006/anbo.1998.0832

Incrocci, L., Massa, D., Carmassi, G., Pulizzi, R., Maggini, R., Pardossi, A., & Bibbiani, C. (2008). SIMULHYDRO, A simple tool for predicting water use and water use efficiency in tomato closed-loop soilless cultivations. In *Acta Horticulturae* (pp. 1005–1012). International Society for Horticultural Science (ISHS), Leuven, Belgium. https://doi.org/10.17660/ActaHortic.2008.801.119

Jones, J. W., Dayan, E., Allen, L. H., Keulen, H. Van, & Challa, H. (1991). A dynamic tomato growth and yield model (t o m g r o). *AmericanSociety of Agricultural Engineers*, *34*(April), 663–672. https://doi.org/10.13031/2013.31715

Kang, M. Z., Cournède, P. H., de Reffye, P., Auclair, D., & Hu, B. G. (2008). Analytical study of a stochastic plant growth model: Application to the GreenLab model. *Mathematics and Computers in Simulation*, *78*(1), 57–75. https://doi.org/10.1016/j.matcom.2007.06.003

Le Bot, J., Adamowicz, S., & Robin, P. (1998). Modelling plant nutrition of horticultural crops: A review. *Scientia Horticulturae*. https://doi.org/10.1016/S0304-4238(98)00082-X

Lemaire, S., Maupas, F., Cournède, P.-H., & De Reffye, P. (2008). A morphogenetic crop model for sugar-beet (Beta vulgaris L.). *International Symposium on Crop Modeling and Decision Support ISCMDS*, *5*, 19–22. https://doi.org/10.1007/978-3-642-01132-0_14

Lizarraga, A., Boesveld, H., Huibers, F., Robles, C., (2003). Evaluating irrigation scheduling of hydroponic tomato in Navarra, Spain. Irrig. and Drain.52: 177-188. Doi:10.1002/ird.86

Martínez-Ruiz, A., López-Cruz, I. L., Ruiz-García, A., & Ramírez-Arias, A. (2012). Calibración y validación de un modelo de transpiración para gestión de riegos de jitomate (Solanum lycopersicum L.) en invernadero *Revista Mexicana de Ciencias Agrícolas*, (4), 757–766.

Massa, D., Incrocci, L., Maggini, R., Bibbiani, C., Carmassi, G., Malorgio, F., & Pardossi, A. (2011). Simulation of crop water and mineral relations in greenhouse soilless culture. *Environmental Modelling and Software*, *26*(6), 711–722. https://doi.org/10.1016/j.envsoft.2011.01.004

Medrano, E., Alonso, F. J., Cruz Sánchez-Guerrero, M., & Lorenzo, P. (2008). Incorporation of a model to predict crop transpiration in a commercial irrigation equipment as a control method for water supply to soilless horticultural crops. In *Acta Horticulturae* (Vol. 801 PART 2, pp. 1325–1330). https://doi.org/10.17660/ActaHortic.2008.801.162

Medrano, E., Lorenzo, P., Sánchez-Guerrero, M. C., & Montero, J. I. (2005). Evaluation and modelling of greenhouse cucumber-crop transpiration under high and low radiation conditions. *Scientia Horticulturae*, *105*(2), 163–175. https://doi.org/10.1016/j.scienta.2005.01.024

ISSN: 2410-3462

Medrano, E., Alonso, F. J., Lorenzo, P., & Sánchez-Guerrero, M. C. (2011). Transpiration and nutrient use efficiency of a sweet pepper crop under two external shading systems: Mobile and fixed. In *Acta Horticulturae* (Vol. 893, pp. 945–952). https://doi.org/10.17660/ActaHortic.2011.893.106

Mengel, Konrad; Kirkby, Ernest A.; Kosegarten, Harald; Appel, T. (2001). *Principles of Plant Nutrition. Soil Science*. https://doi.org/10.1097/00010694-198407000-00012

Montero, J. I., Antón, A., Muñoz, P., & Lorenzo, P. (2001). Transpiration from geranium grown under high temperatures and low humidities in greenhouses. *Agricultural and Forest Meteorology*, *107*(4), 323–332. https://doi.org/10.1016/S0168-1923(01)00215-5

Orgaz, F., Fernández, M. D., Bonachela, S., Gallardo, M., & Fereres, E. (2005). Evapotranspiration of horticultural crops in an unheated plastic greenhouse. *Agricultural Water Management*, *72*(2), 81–96. https://doi.org/10.1016/j.agwat.2004.09.010

Peet, M., & Welles, G. (2005). Greenhouse tomato production. Heuvelink, E.P. (Ed.), Crop Production Science. Horticulture Series. https://doi.org/10.1016/j.jenvman.2008.06.006

Reffye, P., Heuvelink, E., Guo, Y., Hu, B. G., & Zhang, B. G. (2009). Coupling process-based models and plant architectural models: A key issue for simulating crop production. *Crop Modeling and Decision Support*, *4*, 130–147. 10.1007/978-3-642-01132-0_15

Sergio, A. Gabriel, Z. Javier, A. Enrique, G. Diego, & L., I. (2003). Terra Latinoamericana. *Terra Latinoamericana*, *21*, 177–183.

Shibu, M. E., Leffelaar, P. A., van Keulen, H., & Aggarwal, P. K. (2010). LINTUL3, a simulation model for nitrogen-limited situations: Application to rice. *European Journal of Agronomy*, *32*(4), 255–271. https://doi.org/10.1016/j.eja.2010.01.003

Soltani, A. Sinclair, T. R. (2012). *Modeling physiology of crop development, growth and yield. Growth and Yield. CABI publication. 322p*. https://doi.org/10.1079/9781845939700.0102

Steiner, A. A. (1980). The selective capacity of plant for ions and its importance for the composition and treatment of the nutrient solution, Acta Horticulturae.98. https://doi.org/10.17660/ActaHortic.1980.98.7

Stockle, C. O., Donatelli, M., & Nelson, R. (2003). CropSyst, a cropping systems simulation model. *European Journal of Agronomy*, *18*, 289–307. https://doi.org/Pii S1161-0301(02)00109-0

Stockle, C. O., Martin, S. A., & Campbell, G. S. (1994). CropSyst, a cropping systems simulation model: Water/nitrogen budgets and crop yield. *Agricultural Systems*, *46*(3), 335–359. https://doi.org/10.1016/0308-521X(94)90006-2

Ta, T. H., Shin, J. H., Ahn, T. I., & Son, J. E. (2011). Modeling of transpiration of paprika (Capsicum annuum L.) plants based on radiation and leaf area index in soilless culture. *Horticulture Environment and Biotechnology*, *52*(3), 265–269. https://doi.org/10.1007/s13580-011-0216-3

Tei, F., Benincasa, P., & Guiducci, M. (2002). Effect of n availability on growth, n uptake, light interception and photosynthetic activity in processing tomato. In *Acta Horticulturae* (pp. 209–216). International Society for Horticultural Science (ISHS), Leuven, Belgium. https://doi.org/10.17660/ActaHortic.2002.571.25

Thornley, J.H.M. and France J. (2007)**.** Mathematical models in Agriculture. Quantitative Methods for the Plant, Animal and Ecological Sciences. CABI. 905 pp.

ISSN: 2410-3462

Vazquez-Cruz, M. A., Guzman-Cruz, R., Lopez-Cruz, I. L., Cornejo-Perez, O., Torres-Pacheco, I., & Guevara-Gonzalez, R. G. (2014). Global sensitivity analysis by means of EFAST and Sobol' methods and calibration of reduced state-variable TOMGRO model using genetic algorithms. *Computers and Electronics in Agriculture*, *100*, 1–12. https://doi.org/http://dx.doi.org/10.1016/j.compag.2013.10.006

Xu, R., Dai, J., Luo, W., Yin, X., Li, Y., Tai, X., … Diao, M. (2010). A photothermal model of leaf area index for greenhouse crops. *Agricultural and Forest Meteorology*, *150*(4), 541–552. https://doi.org/10.1016/j.agrformet.2010.01.019

ISSN: 2410-3462

Article **Journal Simulation and Laboratory**
December 2022 Vol.9 No.27 14-19

Control of a CNC laser engraver machine for non-metallic materials

Control de una maquina CNC grabador láser para materiales no metálicos

PACHECO-ALVARADO, Luis Kevin†*, GONZALEZ-MONZON, Ana Lilia, PIÑA-ALCANTARA Henry Christopher and TORRES-ARREOLA, León Guillermo

Tecnológico de Estudios Superiores de Jilotepec, México

ID 1st Author: *Luis Kevin, Pacheco-Alvarado* / **ORC ID:** 0000-0002-0722-1346, **CVU CONACYT ID**: 883154

ID 1st Co-author: *Ana Lilia, González-Monzón* / **ORC ID:** 0000-0002-0280-0525, **CVU CONACYT ID**: 151293

ID 2nd Co-author: *Henry Christopher, Piña-Alcantara* / **ORC ID:** 0000-0001-5726-2915, **CVU CONACYT ID**: 719620

ID 3rd Co-author: *León Guillermo, Torres-Arreola* / **ORC ID:** 0000-0002-7694-9613, **CVU CONACYT ID**: 1205387

DOI: 10.35429/JSL.2022.27.9.14.19 Received July 30 2022; Accepted December 30, 2022

Abstract

The present work consists of the development of a control system by means of a microprocessor for a prototype of engraving of non-metallic materials using a semiconductor laser, which has the purpose of carrying out said process without the use of any image processing software as they do. other common marketing devices. This prototype is based on a Cartesian positioning robot, built with a 20mm structural aluminum profile, a 450nm wavelength laser module at 1W of power adjustable by PWM pulse width modulation, 3 motors with Nema 17 bipolar steps, an ATMega2560 microcontroller and a CNC shield card. As a result, we obtain a prototype of a laser engraver with a microcontroller control system, which according to the tests carried out has an efficiency of 95%, capable of carrying out a maximum of 27 engraving processes every 60 minutes with a 30-minute break and that does not use image processing software.

Microcontroller, CNC, Control

Resumen

El presente trabajo consiste en el desarrollo de un sistema de control mediante un microprocesador para un prototipo de grabado de materiales no metálicos utilizando un láser de semiconductor, que tiene el propósito realizar dicho proceso sin el uso de algún software de procesamiento de imágenes como lo hacen otros dispositivos de comercialización común. Este prototipo está basado en un robot de posicionamiento cartesiano, construido con perfil de aluminio estructural de 20mm, un módulo láser de 450nm de longitud de onda a 1 W de potencia regulable mediante modulación de ancho de pulso PWM por sus siglas en inglés, 3 motores a pasos bipolares Nema 17, un microcontrolador ATMega2560 y una tarjeta CNC shield. Como resultado obtenemos un prototipo de grabador láser con un sistema de control mediante microcontrolador, que según las pruebas realizadas tiene una eficiencia del 95%, capaz de realizar un máximo de 27 procesos de grabado cada 60 minutos con 30 minutos de descanso y que no utiliza un software de procesamiento de imágenes.

Microcontrolador, CNC, Control

Citation: PACHECO-ALVARADO, Luis Kevin, GONZALEZ-MONZON, Ana Lilia, PIÑA-ALCANTARA Henry Christopher and TORRES-ARREOLA, León Guillermo. Control of a CNC laser engraver machine for non-metallic materials. Journal Simulation and Laboratory. 2022, 9-27: 14-19

*Correspondence to Author (e-mail: ing.kpacheco@hotmail.com)
†Researcher contributing as first Author.

Introduction

Currently, there are a number of machines on the market that perform engraving and cutting processes of metallic and non-metallic materials by means of working tools that can vary according to the type of device and according to the needs and demands of the customers. There are systems that work using roughing as a process of transformation of materials and there are other processes such as steaming that offer the possibility of having greater precision in the engraving or cutting.

In a constant process of innovation for the improvement of techniques for the manufacture of raw materials, we have worked hard to increase productivity and greater precision in the work performed. The best known techniques are: turning, drilling, planing, grinding, milling and scribing, just to mention a few.

The worldwide dynamics of globalization in production presents us with the great need to automate these material manufacturing techniques in order to reduce time and eliminate some errors that can become common due to human intervention, as well as to achieve greater productivity and precision. This can be possible thanks to Computer Numerical Control (CNC) machines, which is complemented with an abrasive tool.

This work addresses the implementation of a microcontroller control system for an engraving prototype whose tool is a 450 nm wavelength coherent light emitting diode for non-metallic materials.

Development

For the development of the project, the methodology shown in Figure 1 was used, where it mentions the steps to design and assemble the laser engraver prototype, as well as to develop the control system using a microcontroller.

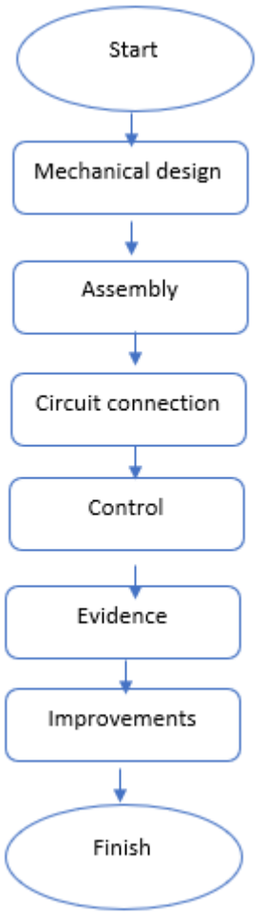

Figure 1 Methodology flowchart
Source (project contribution, unpublished)

Mechanical Design

The laser recording system is a positioner in Cartesian configuration, it has a structure with a 20mm IPS profile, which is formed by a transmission through a toothed belt and plastic wheels with bearings, through stepper motors, it is integrated by several pieces machined in MDF material of 6mm thickness.

Two 20x20 mm by 250 mm long IPS structural profiles are used, which constitute the width of the frame of the main structure of the prototype, two 20x20 mm by 350 mm long IPS aluminum structural profiles are used, which constitute the length of the frame of the main structure of the prototype, also 4 aluminum corner pieces are used as angle supports and as fastening of the aluminum structural profiles described above, together with the 4 square nuts of 3/8" and M5 screws. The representation of the frame of the main structure of the prototype can be seen in Figure 2.

ISSN: 2410-3462

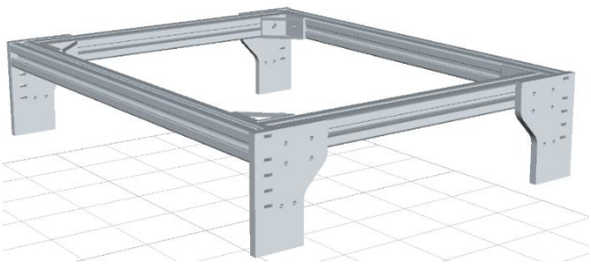

Figure 2 Representation of the base structure of the laser engraver system in CAD software
Source (project contribution, unpublished)

The Y axis of the laser engraver prototype slides directly on the frame of the main structure of the prototype and, unlike the X axis, this one contemplates the use of 2 stepper motors that with their coordinated movements create a uniform displacement.

Figure 3 shows a representation of the Y axis mounted on the frame of the main structure of the laser engraver prototype, drawn in CAD software, the pieces shown in yellow, integrate all the elements that constitute the Y axis.

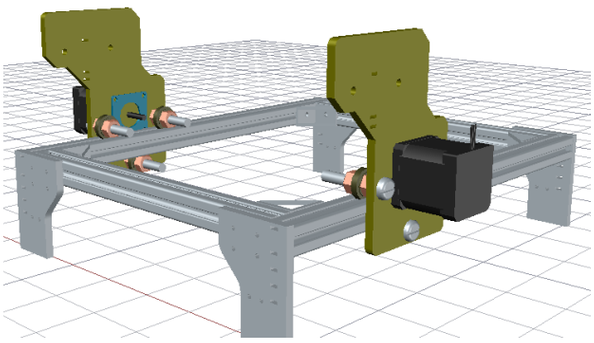

Figure 3 Representation of the Y-axis on the frame of the main structure of the prototype in CAD software
Source (project contribution, unpublished)

In the same way, Figure 4 shows a representation of the mounting of the X axis on the Y axis of the laser engraver prototype of the present work, drawn in CAD software.

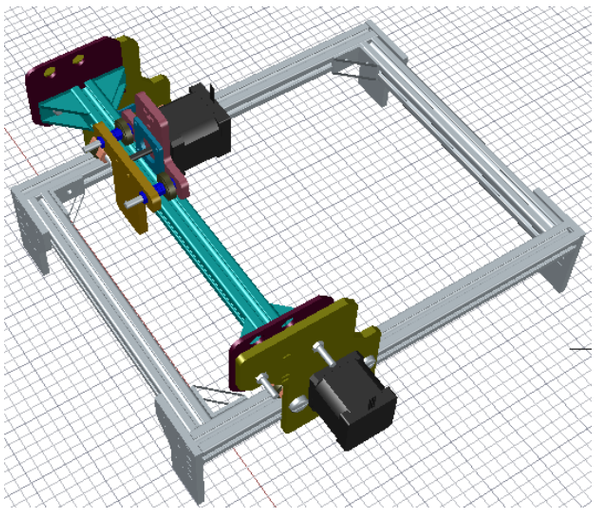

Figure 4 Representation of the X-axis mounted on the Y-axis of the laser engraver prototype in CAD software.
Source (project contribution, unpublished)

Mechanical Assembly

To carry out the mechanical assembly, we used the elements shown in Figure 5, which are half-inch long M5 screws, 2 IPS aluminum structural profiles 20x20 mm by 350 mm long, 2 IPS aluminum structural profiles 20x20 mm by 250 mm long, 4 angled aluminum corner pieces and 3/8-inch square nuts for M5 screws and Nema 17 stepper motors.

Figure 5 Prototype laser engraver with 2 axes and main structure
Source (project contribution, unpublished)

Circuit connection of the laser engraver prototype

The connection of the circuits of the laser engraver prototype can be seen in Figure 6, which has two 12V power supplies, one source will serve for the control system integrated by the microcontroller, the other source supplies power to the drivers and stepper motors.

ISSN: 2410-3462

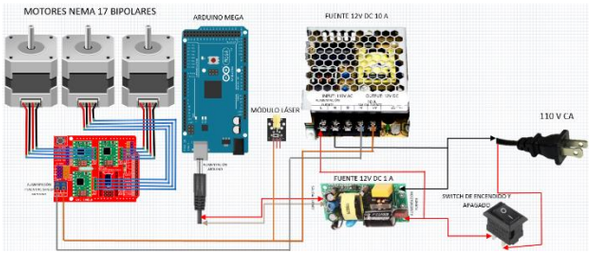

Figure 6 Connection diagram of the laser engraving system
Source (project contribution, unpublished)

Laser engraver prototype control.

The Nema 17 stepper motor used in the laser engraver prototype has an axis of 5 mm in diameter by 20 mm long and for each step it advances 1.8 degrees, where it is necessary to make 200 steps per turn.

To transmit the movement of the motors to the shaft structure and generate displacement, a mechanism was used that consists of integrating a GT2 toothed pulley with 20 teeth and placing it in front of a toothed belt 6 mm wide and 1.38 mm high for the same type of toothed pulley with a tooth height of 0.75 mm, based on Figure 7.

Figure 7 Dimensions of the GT2 20T sprocket given in mm
Source (project contribution, unpublishe)

Having the information of the stepper motor rotation ratio and its linear displacement, an algorithm was developed to generate the necessary movements to write the words MECATRONICS TESJI, the movements are on the X and Y axis, in addition to controlling the intensity of the laser beam of the laser module by means of pulse width modulation, Figure 8 shows the flow diagram that follows the logic of programming.

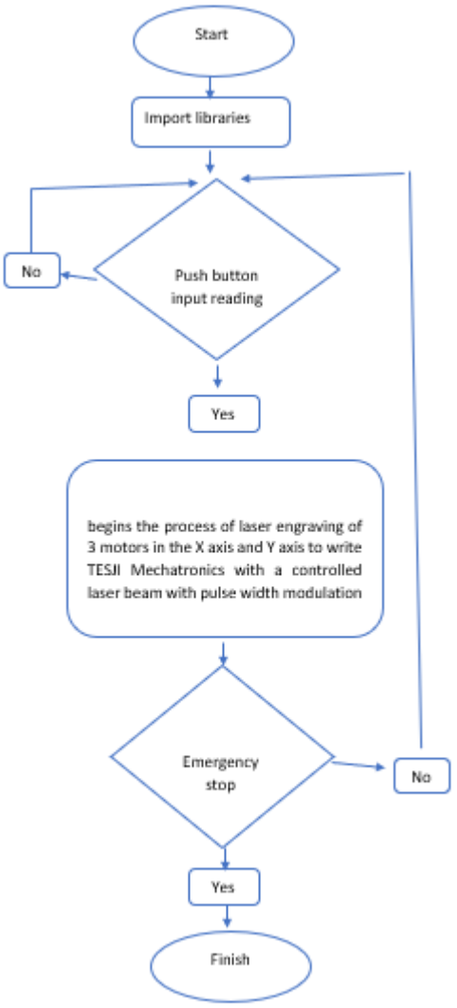

Figure 8 Programming flow chart of the laser engraving system
Source (project contribution, unpublished)

Material tests on the laser engraver

Tests were carried out on different materials to determine the power of laser engraving, using a semiconductor laser module of 1000 mW power and a wavelength of 450 nm. Figure 9 shows the engraving process on 3 mm thick MDF, the material burns accurately without imperfections, and it is a material that has a certain degree of rigidity and flexibility.

Figure 9 Etching test on MDF
Source (project contribution, unpublished)

ISSN: 2410-3462

Another test that was performed was on pine wood, as shown in Figure 10, this test shows certain defects in the recording, due to the properties of the material that is more resistant to incineration, so that in some lines it is not possible to record with adequate precision for visibility.

Figure 10 Pine wood test
Source (project contribution, unpublished)

Laser engraver performance tests

The prototype has been subjected to performance tests over time, so engraving tests have been performed every hour for 5 hours being 25 attempts each hour, in order to know the stability of the system, in addition to knowing the error rate presented in a continuous time, yielding the results captured in Table 1 of performance tests where we obtain a 95.2% final accuracy of the prototype.

Test number	Weather	Type of Error		Percentage of accuracy per test
		Laser head location errors		
1	Hour 1	0	100%	100%
2	Hour 2	0	1	96%
3	Hour 3	0	1	96%
4	Hour 4	0	1	96%
5	Hour 5	1	2	88%
Final prototype accuracy				95.2%

Table 1 Performance tests
Source (project contribution, unpublished)

System improvements and final characterization

Once the tests were carried out, improvements were identified that could enhance the performance of the system. One detail that was improved was the fixing system of the frame where the engravings are made, this was achieved through CAD design and machining as shown in Figure 11.

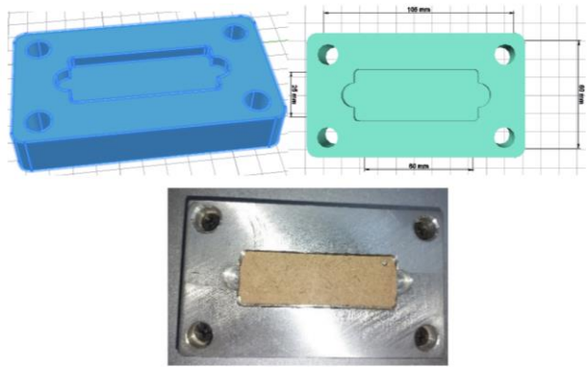

Figure 11 Frame base design in CAD software and final machined part in aluminum
Source (project contribution, unpublished)

We also designed and manufactured the frame holder shown in Figure 12, the height is 150mm to allow 50 recording frames to be placed and the width allows the frames to enter freely without damaging them, it was made of 3mm thick acrylic.

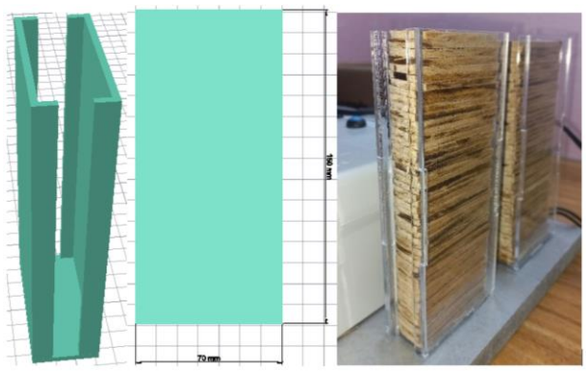

Figure 12 Frame holder design in CAD software and final piece machined in acrylic
Source (project contribution, unpublished)

Finally, a 6mm thick acrylic key ring holder was developed, as shown in Figure 13.

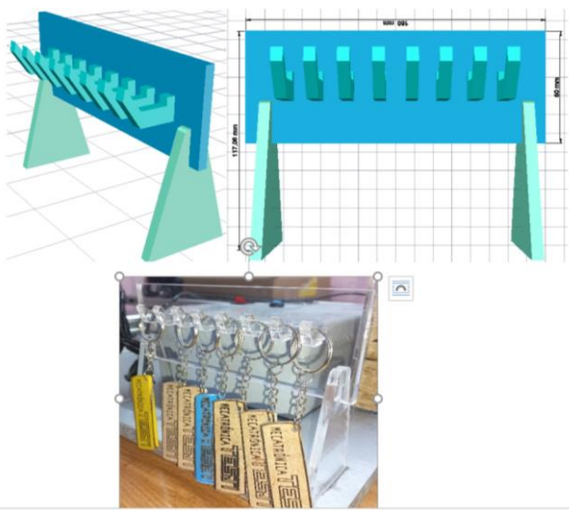

Figure 13 Key holder design in CAD software and final part machined in acrylic
Source (project contribution, unpublished)

ISSN: 2410-3462

Results

Once the improvements to the system have been made, the final characterization of the laser engraver prototype is shown in Figure 14.

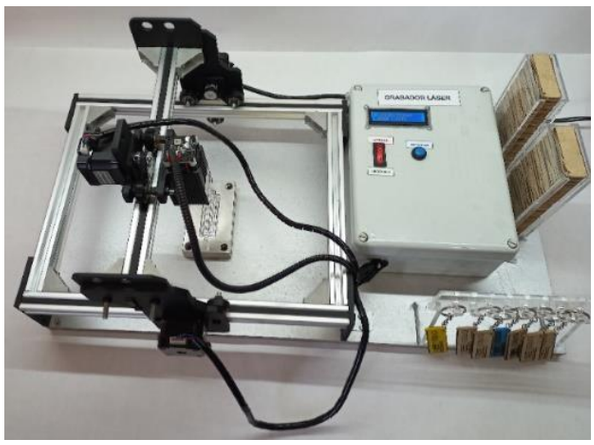

Figure 14 Final characterization of the laser engraving system
Source (project contribution, unpublished)

Considering the tests performed, Graph 1 shows the percentages that occurred during the performance tests and the time interval in which they occurred.

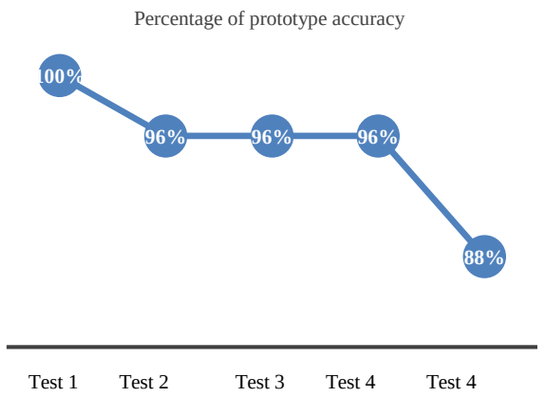

Graph 1 Percentage of accuracy of the prototype
Source (project contribution, unpublished)

As a result of the analysis of the tests performed, an accuracy of 95% was obtained, in addition to proving that the longer the continuous operation time, the more errors it tends to present in its operation, due to the fact that the controllers and the work tool may overheat and thus anomalies may occur in its performance.

Conclusions

By implementing this prototype, it was possible to develop a microcontroller-assisted control system for a laser engraving prototype for non-metallic materials.

It was observed that the time to perform the engraving processes varies according to the material to be used, although the recommendation is the use of MDF where a complete process takes about 2 minutes and 15 seconds; in one hour, the prototype is capable of performing up to 27 processes. When taking the results of the tests and to obtain the highest efficiency and precision of the prototype, it is necessary that after every 60 minutes of work, the prototype has at least 30 minutes of rest, this also based on what is recommended in the data sheets of the DRV8825 controllers and the working tool.

References

Cursar, Q. C. (2021, 5 octubre). Ventajas y desventajas del uso de AutoCAD. Que Cursar.

Camargo Galán, C. E. & Samacá Moreno, I. C. (2021, 29 julio). Diseño y construcción de una cortadora láser para trabajo en 2D.

Hardware Libre, S. W. (2020, 5 mayo). Nema 17: todo sobre el motor paso a paso compatible con Arduino. Hardware libre.

Sarta, J. F. (2020, 1 abril). Calibración del driver DRV8825. Moviltronics.

Delgado, A. L. M. (2020, 14 febrero). Diseño y fabricación de una máquina CNC de corte láser multipropósito.

Zerón, L. Z. (2018, 6 noviembre). Parámetros de una Cortadora Láser para una producción de éxito.

Padilla Ortiz, R. N. (2017, julio). Diseño y construcción de una cortadora láser para papel con interfaz gráfica. Repositorio.UTN.

Chaparro Reyes, L. E. (2017, 1 julio). Localización y Posicionamiento de un Robot Cartesiano en el Centroide de un Objeto.

Chávez Talavera, R. E. (2015, julio). Prototipo cortador y grabador láser. Tesis IPN.

ISSN: 2410-3462

Article **Journal Simulation and Laboratory**
December 2022 Vol.9 No.27 20-28

Analysis of thermoelectrics used in the aerospace industry for power generation by the seebeck effect

Análisis de termoeléctricos utilizados en el sector aeroespacial para la generación de energía mediante efecto seebeck

RODRIGUEZ-AVILA, Jesus*†, VALLE-HERNANDEZ, Julio and GALLARDO-VILLARREAL, José Manuel

Universidad Politécnica Metropolitana de Hidalgo
Universidad Autónoma del Estado de Hidalgo

ID 1st Author: *Jesus, Rodriguez-Avila* / **ORC ID**: 0000-0002-4124-2159, **CVU CONACYT ID**: 1148513

ID 1st Co-author: *Julio, Valle-Hernandez* / **ORC ID**: 0000-0001-8957-0066, **CVU CONACYT ID**: 210743

ID 2nd Co-author: *José Manuel, Gallardo-Villarreal* / **ORC ID**: 0000-0002-7578-7229, **CVU CONACYT ID**: 366394

DOI: 10.35429/JSL.2022.27.9.20.28 Received July 30 2022; Accepted December 30, 2022

Abstract

Currently the generation of energy in space is of vital importance for research on other planets and moons, as all missions sent are powered by electricity so that they keep all their instruments operating properly and present no short-term problems. For the generation of energy outside the planet earth are presented the power converters which are able to convert thermal energy into electrical energy, currently there are two types of power converters which are dynamic and static, for this work are addressed the static, also called thermoelectric that work from a physical phenomenon called seebeck effect which USES two metals of different composition united, They take advantage of a temperature gradient where one end is kept at a hot temperature and the other at a cold temperature, causing a voltage differential. For a material to be considered thermoelectric and work properly has to have some properties such as the seebeck coefficient, electrical resistivity and thermal conductivity, in this work we study some thermoelectrics used in the aerospace sector which are Bi_2Te_3, $PbTe$, $SiGe$, Skutterudite and $BiSbTe$ Where its thermoelectric properties will be analyzed according to its operating temperature range, the merit figure zt will be calculated, the electrical power generated, the input heat and the output heat, finally a comparative table of the electrical power generated by the static converters and another of its applications in the space sector will be performed. This work provides information on the most used thermoelectrics in the space sector, as well as the physical phenomena involved in static converters.

Thermoelectric, Merit Chart, Seebeck coefficient

Resumen

Actualmente la generación de energía en el espacio es de vital importancia para la investigación en otros planetas y lunas, ya que todas las misiones enviadas son alimentadas por electricidad de forma que mantengan todos sus instrumentos operando de manera adecuada y no presente problemas a corto plazo. Para la generación de energía fuera del planeta tierra se presentan los convertidores de potencia los cuales son capaces de convertir la energía térmica en energía eléctrica, actualmente existen dos tipos de convertidores de potencia los cuales son los dinámicos y los estáticos, para este trabajo se abordan los estáticos, también llamados como termoeléctricos que funcionan a partir de un fenómeno físico llamado efecto Seebeck el cual utiliza dos metales de diferente composición unidos, estos aprovechan un gradiente de temperatura donde un extremo se mantiene a una temperatura caliente y otro a una temperatura fría, ocasionando un diferencial de voltaje. Para que un material sea considerado termoeléctrico y funcione correctamente tiene que presentar algunas propiedades como el Coeficiente de Seebeck, Resistividad Eléctrica y la Conductividad Térmica, en este trabajo se estudiaran algunos termoeléctricos utilizados en el sector aeroespacial los cuales son Bi_2Te_3, $PbTe$, $SiGe$, Skutterudite y $BiSbTe$ donde se analizara sus propiedades termoeléctricas de acuerdo a su rango de temperatura de operación, se calculara la figura de mérito ZT, la potencia eléctrica generada, el calor de entrada y el calor de salida, finalmente se realizara una tabla comparativa de la potencia eléctrica generada por los convertidores estáticos y otra de sus aplicaciones en el sector espacial. Este trabajo brinda información sobre los termoeléctricos mas utilizados en el sector espacial, así como los fenómenos físicos involucrados en los convertidores estáticos.

Termoeléctrico, Grafica de Merito, Coeficiente de Seebeck

Citation: RODRIGUEZ-AVILA, Jesus, VALLE-HERNANDEZ, Julio and GALLARDO-VILLARREAL, José Manuel. Analysis of thermoelectrics used in the aerospace industry for power generation by the seebeck effect. Journal Simulation and Laboratory. 2022, 9-27: 20-28

*Correspondence to Author (email: aracelih@icf.unam.mx)
†Researcher contributing as first Author.

1. Introduction

Power generation for the aerospace sector is very important nowadays since it represents an important point for any mission that requires electrical power supply in order to maintain all its scientific instruments and components that help its movement through space, with the purpose of proper operation. There are several ways to generate electrical energy in space is by means of solar panels that are placed externally attached to the structure of the aircraft or deployed to collect light from the sun to later convert it into electrical energy, this process is known as photovoltaic effect.

On the other hand, the use of nuclear energy in space has been present since the last decade in missions where distances are so far away that sunlight cannot reach with the same intensity, so nuclear energy in space requires dynamic and static power converters. Static converters do not require any moving parts for their operation, these converters are also called thermoelectric, there are three types of thermoelectric effects which have various applications in the generation of electric potentials through the Seebeck effect and cooling of small volumes using the Peltier effect. These thermoelectric effects are classified into Seebeck, Peltier and Thomson effect. The Peltier effect, the opposite of the Seebeck effect, consists of supplying an electric current in an electric circuit formed by two different metals, in one of its junctions heat will be absorbed from the medium and in the other it will be given up. In this effect the ratio of current supplied for cooling is directly proportional to the temperature difference between the junctions of the two metals.

The Thomson effect is described as the absorption or generation of heat along a homogeneous electrical conductor, through which an electric current flows and with junctions at different temperatures. In other words, the heat is proportional to the electric current and the temperature gradient.

For the Seebeck effect a closed circuit composed of two different metals in contact, with junctions at different temperatures, generates an electric current which has as a consequence a magnetic field, which was detected by a galvanometer, which Seebeck had close to the circuit.

Consequently, in an open circuit, under the same conditions, an electric potential difference is generated in its junctions. The relationship between the temperature gradient and the voltage generated is direct, and is related to the proportionality constant called Seebeck's coefficient (S). The thermoelectrics to be analyzed for this work are Bi_2 Te_3, PbTe, Skutterudite, BiSbTe and SiGe, making them viable candidates for implementation in the aerospace sector.

According to the thermoelectrics proposed for this work, some properties are obtained in the form of polynomials such as Seebeck coefficient, electrical resistivity and thermal conductivity, from these properties, the input and output thermal power is calculated, then the electrical power generated by the thermoelectrics is determined with an energy balance. With the results obtained it is determined that they would have in the aerospace sector.

2. Methodology

This work has the following methodology to be developed:

– Thermoelectric by Seebeck effect.
– Polynomials for thermoelectric types by Seebeck effect.
– Calculate the Seebeck coefficient, electrical resistivity and thermal conductivity as a function of thermoelectric temperature ranges.
– Calculate the electrical power generated by each type of thermoelectric power plant.
– Seebeck effect thermoelectrics applications in space.

3. Development

In the following section the development for the analysis of the different thermoelectrics used in the space sector is carried out. For this purpose, a search for the best thermoelectrics with the best properties such as Seebeck Coefficient, electrical resistivity and thermal conductivity was carried out in order to analyze them separately according to their operating temperature range.

ISSN: 2410-3462

3.1. Static Power Converters

Thermoelectric generators are solid-state devices with no moving parts, reliable and scalable solid-state devices, which are ideal for small-quantity power generation and energy harvesting. Thermoelectric generators (TEGs), known as solid-state devices, are used to generate electrical power from a temperature gradient. TEGs are small in size and maintenance-free.

To generate electricity through the thermoelectric effect, a thermoelectric module and a temperature difference between the two sides of the module are required. Since current circulation also generates heat migration, the hot and cold sources must continuously contribute and dissipate heat to maintain this difference. A thermoelectric module generally consists of three to 127 pairs; the pairs are connected together electrically in series and thermally in parallel to form the device.

The thermoelectric system is composed of modules of different semiconductor materials because the performance changes with operating temperature.

The materials selected for the thermoelectric system are Bismuth Telluride (Bi_2 T_3), Lead Telluride (PbTe), Silicon Germanium (SiGe), Bismuth Antimony Telluride (BiSbTe) and Skutterudite. Thermoelectrics have different temperature ranges, which are described as follows.

Static Power Converters	
Thermoelectric	Operating Temperature Range
Bismuth Telluride	300 a 570 K
Lead Telluride	500 a 800 K
Silicon Germanium	750 a 1000 K
Skutterudite	273 a 773 K
Bismuth Telluride Antimony	273 a 773 K

Table 1 Temperature Range Thermoelectrics

Due to their composition and temperature range, they present significant changes in some thermal and electrical properties in some thermal and electrical properties.

The efficiency of thermoelectric devices is very strongly associated with a figure of merit dimension in Eq.1.

$$\mathrm{ZT} = \frac{S^2\sigma}{k}T \tag{1}$$

Where:

ZT = Figure of merit.
S = Coeficiente de Seebeck $\left[\frac{V}{K}\right]$.
σ = Electrical Conductivity $\left[\frac{1}{\Omega m}\right]$.
k = Thermal conductivity $\left[\frac{W}{mK}\right]$.
T = Absolute temperature $[K]$.

The ZT figure is also a convenient indicator for the evaluation of the potential efficiency of thermoelectric devices: a good thermoelectric material has, in general, a ZT value close to unity. Static power converters usually have a low efficiency.

3.2 Thermoelectric Properties

In order to calculate the electrical power generated, it is necessary to know the thermoelectric properties, which are as follows:

Seebeck coefficient (S, $\left[\frac{V}{K}\right]$).
Electrical Resistivity (ρ, $[\Omega m]$).
Electrical Conductivity (k, $\left[\frac{W}{mK}\right]$).
Electrical Resistance (R, $[\Omega]$)
Electric Current (I, $[A]$).

Bismuth telluride has a low temperature range compared to the other selected thermoelectrics so the values corresponding to the Seebeck coefficient, thermal conductivity and electrical conductivity are taken by means of the following polynomials obtained from the experimental values of reference [III][IV]. The polynomial of the Seebeck coefficient and the electrical resistivity (ρ) of the thermoelectric Bi_2 Te_3 is a function of the temperature range to determine it, it is necessary to take the temperature in Kelvin from 300K to 570K, which is expressed in the following polynomials la Ec.2 y Ec.3.

$$\mathrm{S(T_s)} = -1.9 * 10^{-6}T_s^5 - 0.12 * 10^{-6}T_s^4 + 4.1 * 10^{-6}T_s^3 - 3.4 * 10^{-6}T_s^2 + 11 * 10^{-6}T_s + 1.5 * 10^{-6} \tag{2}$$

$$\rho(\mathrm{T}_\rho) = 2.5 * 10^{-7}\mathrm{T}_\rho{}^2 + 2.7 * 10^{-6}\mathrm{T}_\rho + 4.1 * 10^{-5} \tag{3}$$

ISSN: 2410-3462

Where the value of z is expressed as the Ec.4.

$$T_s = T_\rho = \frac{T-4.1*10^2}{76} \quad (4)$$

In this case the thermal conductivity remains constant for the temperature range used, around 0.85 W/(m*K) [III]. For the PbTe material according to a temperature range from 500K to 800K, the following polynomials of experimental values were obtained from the reference [III][V].

$$S(T_s) = -8.2*10^{-6}{T_s}^4 - 7.3*10^{-6}{T_s}^3 - 7.9*10^{-6}{T_s}^2 + 54*10^{-6}T_s + 2.8*10^{-4} \quad (5)$$

$$\rho(T_\rho) = 6.4*10^{-5}T_\rho + 5.5*10^{-5} \quad (6)$$

$$k(T_k) = 0.23*{T_k}^2 - 0.28*T_k + 1.2 \quad (7)$$

Where the values of T_s,T_ρ and T_k are expressed in the following equations:

$$T_s = \frac{T-5.3*10^2}{150} \quad (8)$$

$$T_\rho = \frac{T-5.3*10^2}{350} \quad (9)$$

$$T_k = \frac{T-5.3*10^2}{170} \quad (10)$$

For the SiGe thermoelectric, which is in the higher operating temperature range from 750K to 1000K, the polynomials corresponding to its properties are expressed according to experimental values from the references [III][VI].

$$S(T_s) = -4.5*10^{-6}{T_s}^3 - 9.6*10^{-6}{T_s}^2 + 6*10^{-5}T_s + 0.0002 \quad (11)$$

$$\rho(T_\rho) = 1/(8.7*10^3{T_\rho}^2 - 2.5*10^4T_\rho + 6.7*10^4) \quad (12)$$

Where the values for T_s y T_ρ are expressed in the following equations:

$$T_s = \frac{T-6.5*10^2}{240} \quad (13)$$

$$T_\rho = \frac{T-6.5*10^2}{240} \quad (14)$$

The thermal conductivity of SiGe over the temperature range used is practically constant, $4.5\frac{W}{m*K}$[III].

The thermoelectric properties of Skutterudite are given in the form of a polynomial, taking into account that the temperature must be in degrees Celsius. [VI][VII]. The polynomials obtained are as follows.

$$S(T_s) = -1.06*10^{-4} - 2.92*10^{-7}T_s + 2.24*10^{-10}{T_s}^2 \quad (15)$$

$$\rho(T_\rho) = 3.25*10^{-6} - 5.19*10^{-9}T_\rho - 2.61*10^{-12}{T_\rho}^2 \quad (16)$$

$$k(T_k) = 5.53 - 0.009T_k - 2.45*10^{-5}{T_k}^2 + 3.99*10^{-7}{T_k}^3 + 1.05*10^{-9}{T_k}^4 - 1.4*10^{-11}{T_k}^5 + 1.04*10^{-14}{T_k}^6 + 1.36*10^{-16}{T_k}^7 - 3.66*10^{-19}{T_k}^8 + 2.74*10^{-22}{T_k}^9 \quad (17)$$

For the thermal conductivity, a ninth degree polynomial has been used, where the temperature T is given in °C.

$$T_s = T_k = T_\rho = T \quad (18)$$

On the other hand, the thermoelectric properties of BiSbTe have been obtained from reference [VI][VII], and therefore the following polynomials are obtained.

$$S(T_s) = 1.72*10^{-4} + 5.88*10^{-7}T_s - 1.87*10^{-9}{T_s}^2 \quad (19)$$

$$\rho(T_\rho) = 6.65*10^{-6} + 4.92*10^{-8}T_\rho + 3.14*10^{-11}{T_\rho}^2 \quad (20)$$

$$k(T_k) = 1.21 - 3.71*10^{-3}T_k + 1.60*10^{-5}{T_k}^2 \quad (21)$$

Where the temperature is used according to its operating range in degrees Celsius.

With the Seebeck coefficient (S) of each of the thermoelectrics, the voltage produced is obtained according to the temperature range of each thermoelectric and a temperature on the cold side.

ISSN: 2410-3462

The temperature on the cold side is affected by the hot side, as well as the cooling or dissipation systems in which the phenomena of natural or forced convection and radiation are involved, for this work a temperature is set on the cold side for each of the thermoelectrics. The voltage produced by the semiconductors is obtained according to the principle of the Seebeck effect shown in the Ec.22.

$$\mathrm{V} = \mathrm{S}(T_c - T_f) \tag{22}$$

Where:

V = Voltage $[V]$.
S = Seebeck Coefficient $\left[\frac{V}{K}\right]$.
T_c = Temperature on the hot face $[K]$.
T_f = Cold face temperature $[K]$.

The electrical resistance of the thermoelectrics is determined with the Ec.23.

$$\mathrm{R} = \rho\frac{e}{A} \tag{23}$$

Where:

ρ = Electrical Resistivity $[\Omega * m]$.
e = Thermoelectric thickness $[m]$.
A = Thermoelectric Area $[m^2]$.

The electrical power generated is calculated by means of the Ec.24.

$$\mathrm{P} = \mathrm{SI}\left(\mathrm{T_c} - T_f\right) - RI^2 \tag{24}$$

To obtain the maximum current, the electrical power is partially derived with respect to the current and equaled to zero as shown in the Ec.25.

$$\frac{\partial \mathrm{P}}{\partial \mathrm{I}} = 0 = \mathrm{S}\left(\mathrm{T_c} - T_f\right) - 2RI \tag{25}$$

With the voltage and resistance calculated according to the temperature range of each of the thermoelectrics, the calculation of the maximum electric current is carried out by means of the Ec. 26.

$$I_{max} = \frac{\mathrm{V}}{2R} \tag{26}$$

The calculation of the electrical power generated by thermoelectrics according to their respective temperature ranges, allows to understand which could be their possible applications.

3.3. Electrical Power Calculation

To determine the electrical power generated by thermoelectrics from the input heat (Q_ent), on the hot face (T_c), in a thermoelectric generator, heat conduction, Joule effect and power generation by the Seebeck effect are considered, as shown in equation 27 [III]:

$$\mathrm{Q_{ent}} = ST_cI - \frac{1}{2}RI^2 + \frac{KA(T_c - T_f)}{e} \tag{27}$$

Similarly, the output heat flux (Q_sal) is calculated, considering the above-mentioned effects applied to the wall with the lowest temperature. (T_f).

$$\mathrm{Q_{sal}} = ST_fI + \frac{1}{2}RI^2 + \frac{KA(T_c - T_f)}{e} \tag{28}$$

To determine the electrical power generated by the thermoelectric plant from the heat input and the heat output, an energy balance is used, which is expressed in the following equation.

$$\mathrm{P_e} = \mathrm{Q_{ent}} - \mathrm{Q_{sal}} \tag{23}$$

4. Results

The results obtained are divided into subsections which are made up of the graphs of Seebeck coefficient, electrical resistivity and thermal conductivity of each one of the thermoelectrics, then with the values obtained the corresponding merit graph will be made, the input and output heat will be calculated to later determine the electrical power generated, finally a comparative table of the power generated by the thermoelectrics and their possible applications is shown.

4.1. ZT Figure of Merit

The figure of merit allows to identify the efficiency of the selected thermoelectric plants, as shown in the following graph 1.

ISSN: 2410-3462

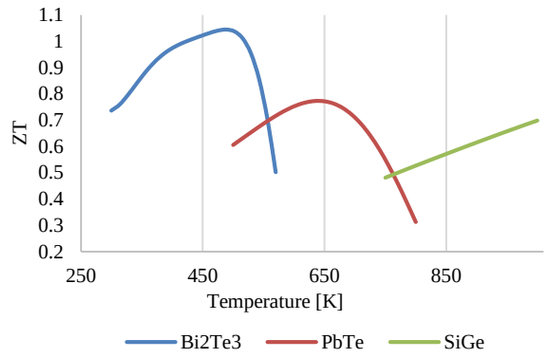

Graph 1 Figure of merit of thermoelectric plants

For the Skutterudite and BiSbTe thermoelectric plants, the following ZT figures of merit are shown in the graph below 2.

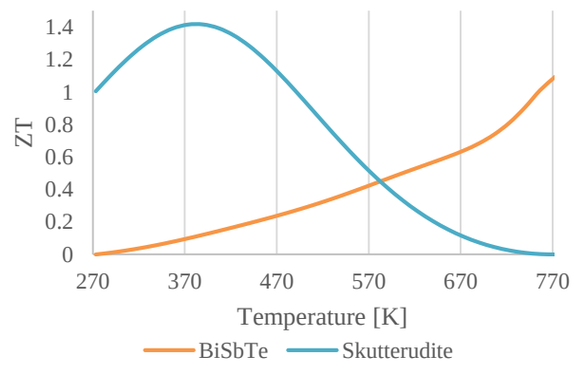

Graph 2 Figure of merit of thermoelectric plants

The selected thermoelectrics have different efficiencies depending on their temperature range, so the higher the ZT, the higher the efficiency.

4.2 Seebeck coefficient

The polynomials obtained from the literature are used to calculate the Seebeck coefficient with the corresponding temperatures, which can be represented in the following graphs.

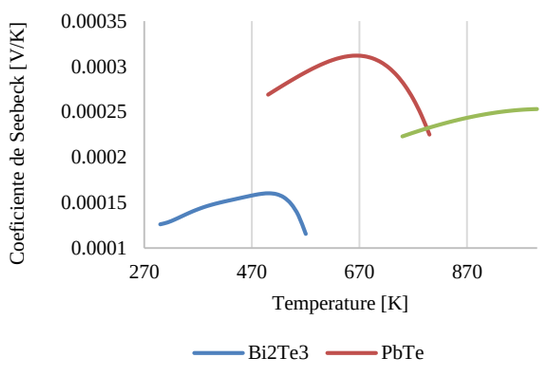

Graph 3 Seebeck Coefficient vs. Bi_2Te_3

For the Seebeck coefficients of the Skutterudite and BiSbTe thermoelectric plants, they have the following ZT figures of merit shown in the chart 2.

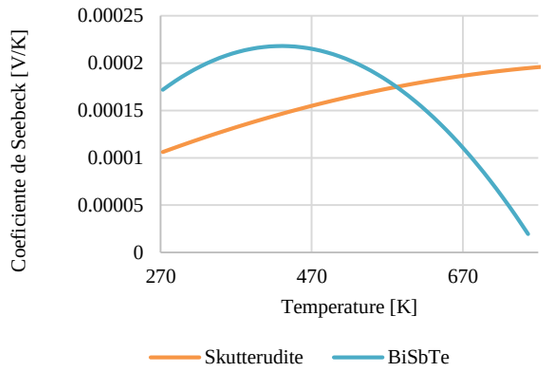

Graph 4 Seebeck Coefficient vs. $PbTe$.

SiGe has the widest temperature range, its coefficient remains relatively high unlike the other thermoelectrics its highest coefficient is at the highest temperature and as the temperature decreases the coefficient decreases.

4.3 Electrical Resistivity

Electrical resistivity refers to a specific point in the material. So what we seek to define is the current density in the resistive material caused. Resistivity, also known as specific resistance of a material is measured in ohms per meter (Ωm). This property changes with respect to the temperature and therefore is different for each thermoelectric, with the polynomials we proceed to make the corresponding graphs shown below.

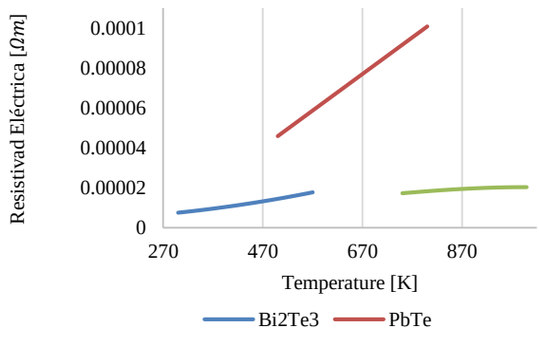

Graph 5 Seebeck Coefficient vs. $PbTe$.

This graph shows that PbTe has a higher electrical resistivity than Bi_2 Te_3 and SiGe. The following graph shows the electrical resistivity of Skutterudite and BiSbTe.

ISSN: 2410-3462

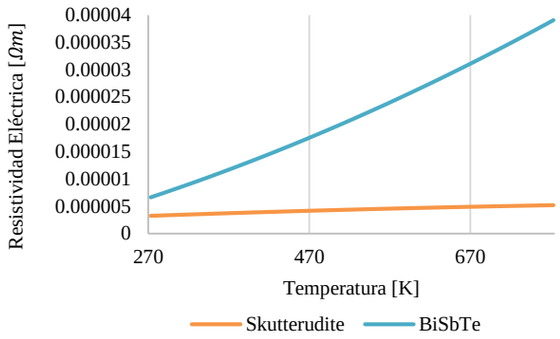

Graph 6 Seebeck Coefficient vs. $PbTe$

It can be observed that unlike the other thermoelectrics analyzed, they have a lower electrical resistivity.

4.4. Thermal Conductivity

Thermal conductivity is important for electrical power calculations, so its polynomials are found as a function of their temperature ranges for some thermoelectrics their thermal conductivity remains constant which are shown in the following table.

Thermal Conductivity	
Thermoelectric	Thermal Conductivity
Bismuth Telluride	$0.85\frac{W}{mK}$
Silicon Germanium	$4.5\frac{W}{mK}$

Table 2 Temperature Range Thermoelectrics

For PbTe, Skutterudite and BiSbTe thermoelectrics, the following plots for thermal conductivity are obtained according to their temperature range.

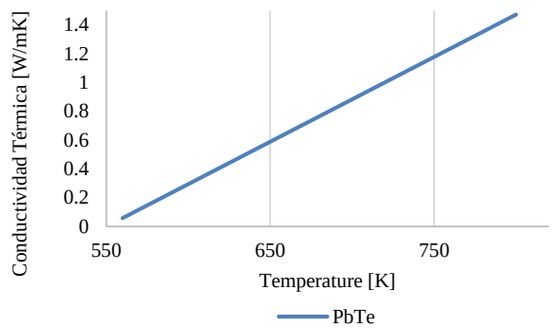

Graph 7 Temperature Range Thermoelectrics

The conductivity varies from 0.05 to 1.47 (W/mK) for PbTe, for the following thermoelectrics are shown in the graph below.

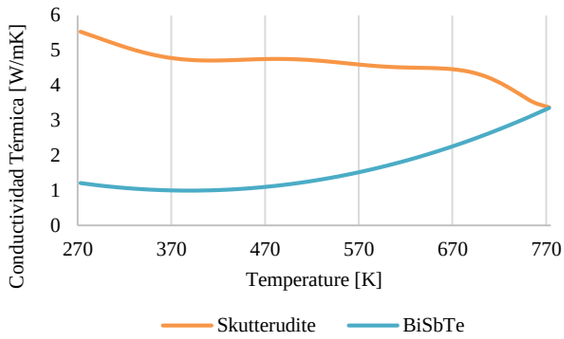

Graph 8 Seebeck Coefficient vs. $PbTe$

It is observed that the Skutterudite thermoelectric has the highest conductivity compared to all the thermoelectrics, with a minimum of 3.37 W/mK and a maximum of 5.53 W/mK.

4.5. Electrical Power

To determine the electrical power is required from the input heat output, it is important to determine the voltage produced, resistance and electrical current. According to Eq.22 the voltage is required a temperature gradient for the hot side in is the operating temperature range, the cold side is influenced by the hot side and by the cooling and radiation systems so it is proposed a temperature for the cold side of the thermoelectric, which is shown in the following table.

Cold Face Temperature	
Thermoelectric	Temperature
Bismuth Telluride	293 K
Lead Telluride	373 K
Silicon Germanium	523 K
Skutterudite	293 K
Bismuth Telluride Antimony	373 K

Table 3 Temperature Range Thermoelectrics

With the temperatures of the cold face, the temperature gradient is substituted in the corresponding equations and the electrical power generated is determined, which is expressed in the following graphs.

ISSN: 2410-3462

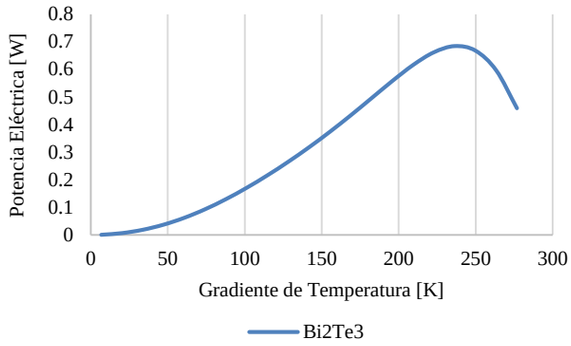

Graph 9 Temperature Range Thermoelectrics

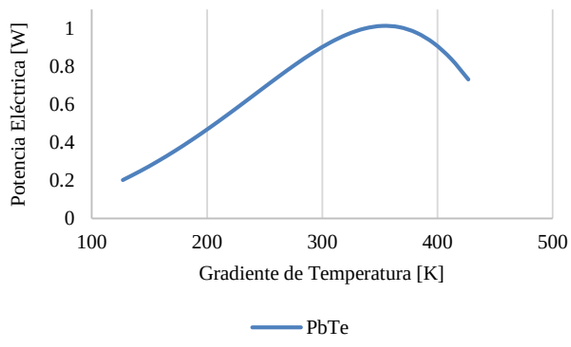

Graph 10 Temperature Range Thermoelectrics

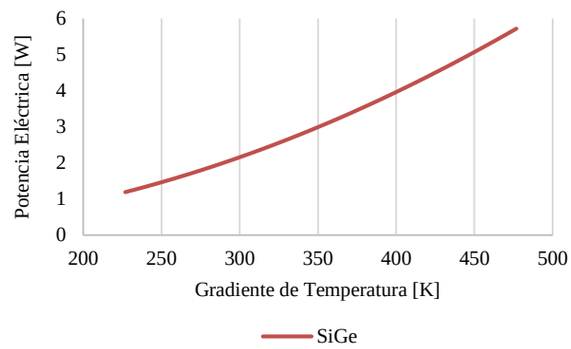

Graph 11 Temperature Range Thermoelectrics

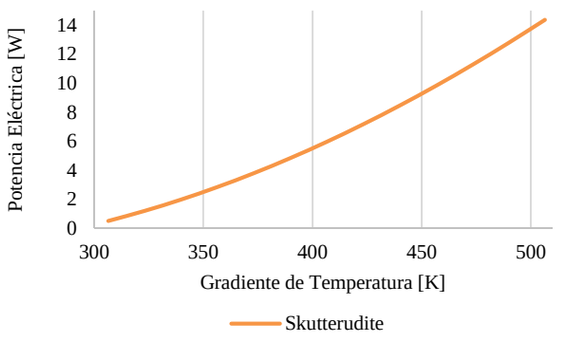

Graph 12 Temperature Range Thermoelectrics.

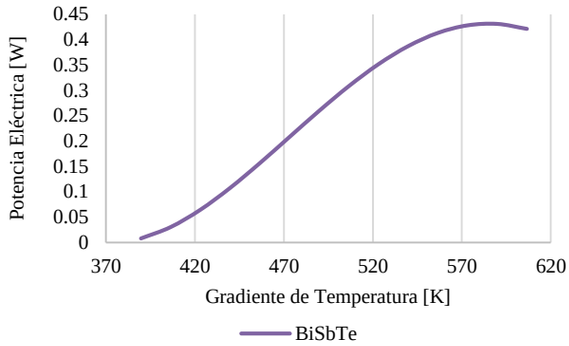

Graph 13 Temperature Range Thermoelectrics

Below is a table with the maximum and minimum values obtained for the electrical power generated with their respective temperature gradient ranges..

Electrical Power Generated [W] [W		
Thermoelectric	Max	Min
Skutterudite	14.4	0.49
$SiGe$	5.7	1.18
$PbTe$	1.0	0.2
Bi_2Te_3	0.68	0.0007
$BiSbTe$	0.43	0.008

It can be seen that the thermoelectric with the highest conversion range is the Skutterudite, so it follows the behavior of the ZT figure of merit as expected, followed by the German Silicon thermoelectric and so on until the end with the BiSbTe which presents the lowest electrical power that has been calculated.

Application	
Thermoelectric	Application
Skutterudite	Low Thermal Power Piping
$SiGe$	Radioisotope Generators and Nuclear Rectors
$PbTe$	Radioisotope Generators
Bi_2Te_3	Radioisotope Generators and Low Power Pipelines
$BiSbTe$	Low Thermal Power Piping

Although Skutterudite has higher efficiency than other thermoelectrics, it is limited by the low operating range, so proper considerations must be made for the implementation of each of the thermoelectrics shown in the paper.

ISSN: 2410-3462

5. Conclusions

It can be seen that the thermoelectric with the highest conversion efficiency is the Skutterudite with a maximum conversion of 14.4W, however its operating temperature range is low so it can only work for systems where the input temperature is low, on the other hand the Germanium Silicon presents a maximum electrical power of 5.7W which shows that although its conversion is low it can work at high temperatures allowing to have a greater flexibility for systems such as radioisotope generators or nuclear reactors for space exploration. On the other hand, it is necessary to take into consideration the phenomena of convection and radiation for the cold side. In conclusion, it is clear that thermoelectrics have a low efficiency, but they can be used in the aerospace sector since they do not have moving or mechanical parts and do not require maintenance, thus allowing their application in various systems where the electrical energy generated by these themselves is not the main source of generation, but works in conjunction with other power conversion systems.

6. Funding

The present work has been funded by CONACYT [grant number: 1148513].

7. References

[1]. Rojas Avila, A. (2020). Estimación de la Energía Eléctrica Aprovechable del Calor Residual de Un Motor Turbofán Mediante un Sistema Termoeléctrico de Efecto Seebeck

[2]. Wu, F., Song, H., Jia, J., & Hu, X. (2013). Effects of Ce, Y, and Sm doping on the thermoelectric properties of Bi2Te3 alloy. Progress in Natural Science: Materials International, 23(4), 408-412.

[3]. Zhu, P., Imai, Y., Isoda, Y., Shinohara, Y., Jia, X., & Zou, G. (2005). Enhanced thermoelectric properties of PbTe alloyed with Sb2Te3. Journal of Physics: Condensed Matter, 17(46), 7319.

[4]. Minnich, A. J., Lee, H., Wang, X. W., Joshi, G., Dresselhaus, M. S., Ren, Z. F., ... & Vashaee, D. (2009). Modeling study of thermoelectric SiGe nanocomposites. Physical Review B, 80(15), 155327.

[6]. González de la Vara, Á. (2017). Análisis por elementos finitos de los generadores termoeléctricos y sus aplicaciones aeroespaciales (Doctoral dissertation, Universitat Politècnica de València).

[7]. Rogl, G., Grytsiv, A., Bauer, E., Rogl, P., & Zehetbauer, M. (2010). Structural and physical properties of n-type skutterudite Ca0. 07Ba0. 23Co3. 95Ni0. 05Sb12. Intermetallics, 18(3), 394-398.

[8]. Poudel, B., Hao, Q., Ma, Y., Lan, Y., Minnich, A., Yu, B., ... & Ren, Z. (2008). High-thermoelectric performance of nanostructured bismuth antimony telluride bulk alloys. Science, 320(5876), 634-638.

ISSN: 2410-3462

Article **Journal Simulation and Laboratory**
December 2022 Vol.9 No.27 29-35

Production of volatile compounds and lipopeptides as antagonistic mechanisms of two *Bacillus* strains towards phytopathogenic fungi

Producción de compuestos volátiles y lipopéptidos como mecanismos antagonistas de dos cepas de *Bacillus* hacia hongos fitopatógenos

RAMÍREZ-MARTÍNEZ, Javier† & PACHECO-AGUILAR, Juan-Ramiro*

Universidad Autónoma de Querétaro, Facultad de Química, Cerro de las campanas s/n, col. Las Campanas, C.P. 76040. Santiago de Querétaro Qro.

ID 1st Author: *Javier, Ramírez-Martínez* / **ORC ID:** 0000-0002-6711-5369, **CVU CONACYT ID:** 1136707

ID 1st Co-author: *Juan Ramiro, Pacheco-Aguilar* / **ORC ID:** 0000-0001-8365-4488, **CVU CONACYT ID:** 87499

DOI: 10.35429/JSL.2022.27.9.29.35 Received July 30 2022; Accepted December 30, 2022

Abstract

Phytopathogenic fungi are one of the main causes of diseases that affect agricultural production. For their control, in recent years, biological alternatives have been developed, such as the use of antagonistic microorganisms that produce inhibitory molecules towards these fungi, exerting a biocontrol effect. In the present study, *Bacillus licheniformis* Q19 and *Bacillus subtilis* Q20 strains were characterized for their ability to inhibit *in vitro* the mycelial growth of *Rhizoctonia solani*, *Fusarium oxysporum*, *Sclerotium rolfsii*, *Colletotrichum gloesporoides* and *Phytophthora* spp. The results of dual cultures show that only Q20 inhibited the pathogens in a range from 33.3 to 50.6 %, being *A. alternata* who presented the greatest inhibition. A positive test for hemolysis, which is related to the lipopeptide production, indicates that these molecules could probably be involved in the fungal inhibition. Later, assays in plates overlapping, where the study microorganisms are not in the same culture médium, showed that Q19 and Q20 produce volatile compunds, capable of inhibiting *A. alternata* and *S. rolfsii* by 72.4 and 56.3 %, respectively. In conclusion, Q19 and Q20 produce lipopeptides and/or volatile compounds with activity against phythopathogenic fungi as biocontrol mechanisms.

Microbial antagonism, Hemolysis, Mycelium

Resumen

Los hongos fitopatógenos, son uno de los principales causantes de enfermedades que afectan la producción agrícola. Para su control, en los últimos años, se han desarrollado alternativas biológicas como es el uso de microorganismo antagonistas que producen moléculas inhibitorias hacia estos hongos, ejerciendo un efecto biocontrol. En el presente estudio, se caracterizaron las cepas de *Bacillus licheniformis* Q19 y *Bacillus subtilis* Q20 en su capacidad para inhibir *in vitro*, el crecimiento micelial de *Rhizoctonia solani*, *Fusarium oxysporum*, *Sclerotium rolfsii*, *Colletotrichum gloesporoides* y *Phytophthora* spp. Los resultados de cultivos duales, muestran que solo Q20 inhibió los patógenos en un rango del 33.3 al 50.6 %, siendo *A. alternata* el que presentó la mayor inhibición. Una prueba positiva de hemólisis, la cual está relacionada con la producción de lipopéptidos, indica que probablemente estas moléculas pudieran estar involucradas en la inhibición. Después, ensayos en placas superpuesta, donde los microorganismos de estudio no se encuentran en el mismo medio de cultivo, mostraron que Q19 y Q20 producen compuestos volátiles, capaces de inhibir a *A. alternata* y *S. rolfsii* en un 72.4 y 56.3 %, respectivamente. En conclusión, Q19 y Q20 producen lipopéptidos y/o compuestos volátiles con actividad hacia hongos fitopatógenos como mecanismos de biocontrol.

Antagonismo microbiano, Hemólisis, Micelio

Citation: RAMÍREZ-MARTÍNEZ, Javier & PACHECO-AGUILAR, Juan-Ramiro. Production of volatile compounds and lipopeptides as antagonistic mechanisms of two *Bacillus* strains towards phytopathogenic fungi. Journal Simulation and Laboratory. 2022, 9-27: 29-35

*Correspondence to Author (e-mail: juanramiro29@yahoo.com.mx)
†Researcher contributing as first Author.

Introduction

Agricultural production in Mexico has been increasing from the 1980s to the present (Baldivia & Ibarra, 2017; SIAP, 2021). However, the phytosanitary problem has always been present, in fact, between 20 and 30% of the annual product from agriculture is affected by pests and/or diseases, where fungi, bacteria, nematodes, as well as viruses and insects are involved (Villarreal *et al*., 2018).

In most cases, postharvest diseases are the limiting factor in fruit and vegetable storage (Benkeblia *et al*., 2011). Mostly, bacterial and fungal species are responsible for the losses of fruits and vegetables in the postharvest period, where the growth of the phytopathogen on the fruit leads to rotting and mycotoxin production by fungal species (Yahaya & Mardiyya, 2019).

For the control of plant pathogenic fungi, broad-spectrum chemical fungicides have conventionally been used to eradicate a large number of pathogenic species. Consequently, the indiscriminate use of these compounds has been negatively affecting soils, ecosystems and human health (Sułowicz & Piotrowska, 2016).

Therefore, the use of sustainable alternatives such as biological control microorganisms or, alternatively, metabolites to mitigate diseases in agricultural crops has been implemented since the last century with great results (Köhl *et al*., 2019).

Bacillus is a bacterial genus that has demonstrated a great antagonistic potential towards phytopathogenic microorganisms, due to its ability to produce antimicrobial compounds including enzymes, antibiotics, lipopeptides and volatile organic compounds (VOCs) (Steinborn *et al*., 2005; Vlot & Rosenkranz, 2022). Among the most studied species with major relevance in agriculture are *B. licheniformis, B. cereus, B. subtilis* and B. *pumilis.*

For example, inhibition of mycelial growth and spore production of plant pathogenic fungi such as *F. oxysporum* by VOCs produced by *B. amyloliquefaciens* has been observed (Yuan *et al*., 2012).

Likewise, Baysal *et al*. (2013), Chaurasia *et al*. (2005) and Yuan *et al*. (2012) reported antagonistic behaviour of VOCs synthesised by *Bacillus* species on common plant pathogen species belonging to the genera *Alternaria, Fusarium, Paecilomyces, Pythium, Rhizoctonia, Aspergillus, Geotrichum, Sclerotinia, Botrytis, Verticillium* and *Colletotrichum.*

In addition, they are also known to produce lipopeptide compounds, which have been shown to antagonise mycelial growth of disease-causing fungi in fruit (Ongena & Jacques, 2008; Rodríguez-Chávez *et al*., 2019; Zhang *et al*., 2022).

On the other hand, the great metabolic diversity among strains of the same species makes it increasingly relevant to search for strains in order to identify new molecules capable of antagonising the growth of phytopathogenic fungi.

Therefore, the aim of the present work was to characterise two *Bacillus* strains in their antagonistic capacity towards phytopathogenic fungi by means of in vitro assays to determine the production of VOCs and/or diffusible lipopeptides in the culture medium.

Methodology to be developed

Biological material

The study strains *B. licheniformis* Q19 and *B. subtilis* Q20 are part of the collection of the company SINQUIMICA, which is dedicated to the commercialisation of biological products. These strains were partially identified by API tests and their biocontrol activity is unknown. The plant pathogenic fungi *Rhizoctonia solani* AG4, *Fusarium oxysporum* FOX13, *Sclerotium rolfsii*, *Colletotrichum gloesporoides* and *Phytophthora spp*. are also part of the SINQUIMICA collection, which are isolated from different regions of the country.

During the experimental work, the bacterial strains were grown on TSA medium and preserved on cellulose filter paper at -20°C. While the fungal strains were subcultured for maintenance on PDA agar in a slant tube and preserved in glycerol at -20°C.

ISSN: 2410-3462

Dual antagonism assays

The dual assays allow to determine the production of diffusible compounds through the medium generating an inhibition halo. For these tests, which were carried out in triplicate, Petri dishes (90 × 15 mm) with PDA were used. A disc (5 mm in diameter) with active mycelium of the plant pathogenic fungus was placed in the centre of the plate and the antagonistic *Bacillus* strain was inoculated 10 mm from the end of the plate by streaking (Shrivastava *et al*., 2017). It should be noted that, due to the doubling time of the bacteria, the bacteria were inoculated 24 h after inoculation of the fungus to allow growth of the fungus.

As a control, PDA plates were used where only the phytopathogenic fungus was seeded. Afterwards, the plates were incubated at 28 °C until the mycelium covered the entire surface of the medium on the control plates, determining the percentage inhibition of radial growth (% ICR) of the fungus and the inhibition halos generated by the bacterial inoculum (Ezziyyani *et al*., 2004).

Detection of lipopeptide production capacity

The bacterial strains were subjected to a haemolysis test on blood agar plates, as strains with lipopeptide production capacity are able to lyse erythrocytes. For this, a fresh culture colony on TSA agar was seeded on blood agar plates, which were incubated 48 h at 37°C, the formation of clearing halos around the colonies was taken as positive for lipopeptide production (Zhao *et al*., 2014).

Confrontation assays on inverted plates

To assess the impact of volatile organic compounds (VOCs) produced by bacterial strains on mycelial growth of plant pathogenic fungi, indirect confrontation assays were carried out on overlapping plates (Abdallah *et al.*, 2018). For this assay, three replicates were carried out for each of the bacterial strains and controls were set up where bacterial inoculation was excepted only growing the plant pathogenic fungus, the completion of the assay was determined when the mycelium covered the entire surface of the medium on the control plates, determining the percentage of inhibition of radial growth of the fungus and the inhibition halos generated by the bacterial inoculum (Ezziyyani *et al*., 2004).

Thus, discs (5 mm in diameter) of active mycelium of the phytopathogenic fungus were seeded in the centre of Petri dishes (90 × 15 mm) with PDA medium and incubated at 28°C for 24h. At the same time, the inoculum of the antagonistic strains was prepared by growing them in Falcon tubes (50 mL, polypropylene) with 20 mL of TSA broth for 24 hours at 35°C and 150 rpm. Upon completion, the bacterial pellet was recovered by centrifugation at 4000 rpm for 10 min, the resulting pellet was washed and resuspended in 10 mL of sterile water to quantify the cell density in a Neubuer chamber. The density was adjusted to $1x10^7$ cell/mL and 150 µL aliquots were inoculated onto TSA plates by extension seeding. The TSA plates were then covered with the PDA plates containing the 24 h fungal growth and Parafilm was used to bind them together, after which they were incubated at 28°C.

Results

Dual antagonism assays

For the exploration of biocontrol effects through compound diffusion by *Bacillus* spp. strains on the different plant pathogenic fungi, the inhibition of radial growth was evaluated (Figure 1). The results showed that strain Q20 reflected better inhibition percentages against most of the phytopathogenic fungi than strain Q19, highlighting the higher antagonism towards A. alternata (Table 1).

.

Mushrooms	*Bacillus* Q19	*Bacillus* Q20
F. oxysporum	6.4 ± 1.9*	41.0 ± 1.3
A. alternata	24.6 ± 3.6	50.6 ± 4.7
C. gloesporoides	4.5 ± 1.6	39.1 ± 2.5
R. solani	7.6 ± 2.9	33.3 ± 3.3
Phytopthora spp.	9.6 ± 1.0	39.1 ± 0.8
S. rolfsii	4.5 ± 3.0	42.2 ± 1.7

* Values are the average of three independent tests. ± Standard deviation.

Table 1 Inhibition percentages of *Bacillus* strains on mycelial growth of plant pathogenic fungi in the dual assay

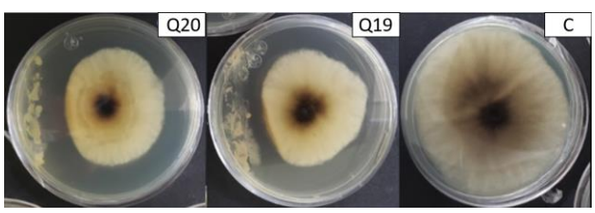

Figure 1 Inhibition of mycelial growth of *A. alternata* in dual antagonism assays with *Bacillus* Q20 and *Bacillus* Q19 strains, control (C).

ISSN: 2410-3462

Lipopeptide production and haemolysis

By this assay, in both *Bacillus* strains, it was possible to detect the production of medium-diffusible compounds with haemolytic capabilities (Figure 2). Although an association between haemolytic activity and lipopeptide production has been reported, further studies are needed to confirm this (Płaza *et al*., 2015; Sarwar *et al*., 2018).

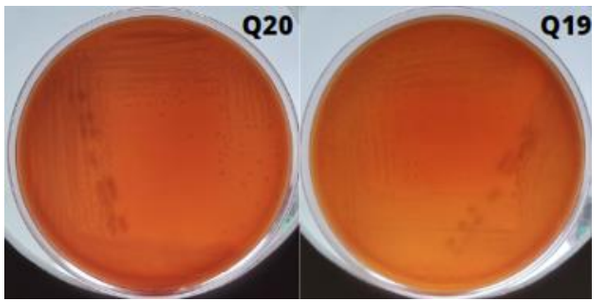

Figure 2 Haemolysis on blood agar plates caused by strains Q20 and Q19, after 24 hours incubation at 37°C.

The inhibitory behaviour of *B. subtilis* and *B. licheniformis* strains against the study pathogens, due to the probable production of lipopeptides, is in agreement with reports by different authors (Qi *et al*., 2010; Romano *et al*., 2013; Ruiz *et al*., 2014; Wang *et al*., 2020). Chaurasia *et al*. (2005) report 66.1 to 71.7 % inhibitory activities of *B. subtilis* (NRRL B-30408) against *A. alternata* and *F. oxysporum*. In addition, Dimkić *et al*. (2013) reported mycelial inhibition towards strains of the genera *Monillinia*, *Penicillium*, *Fusarium*, *Colletotricum* and *Alternaria* through the action of surfactin-like lipopeptides and iturins produced by B. *licheniformis* SS-12.6 and B. *amyloliquefaciens* SS-13.1.

Regarding the mechanism of action of lipopeptide compounds, it is known that particularly, cell wall and fungal cell membrane metabolism are the main processes affected by lipopeptide stress (Zhang *et al*., 2022) ultimately culminating in the induction of apoptosis (Qi *et al*., 2010) or cell lysis (Yu *et al*., 2019). Similarly, the mechanism of action of lipopeptides is known to differ depending on both their peptide and lipid composition (Nasir & Besson, 2012; Yu *et al*., 2019; Zhang *et al*., 2022).

Reversed plate confrontation assays

The percentage mycelial inhibition of plant pathogenic fungi, resulting from the VOCs produced by the study strains, are shown in Table 2. The results indicate that Q19 was able to antagonise mostly *A. alternata* and *S. rolfsii.* While Q20 failed to inhibit *A. alternata* but showed a remarkable ability to inhibit *S. rolfsii* (Figure 3). However, the percentage of inhibition obtained by application of the bacterial treatments to *F. oxysporum* and *R. solai* was the lowest, being less than 20 %.

Mushrooms	*Bacillus* Q19	*Bacillus* Q20
F. oxysporum	10.3 ± 1.9*	18.1 ± 3.5
A. alternata	72.4 ± 3.2	10.8 ± 6.9
C. gloesporoides	31.6 ± 4.8	39.0 ± 5.2
R. solani	2.4 ± 1.0	3.0 ± 1.9
Phytopthora spp.	32.7 ± 1.5	36.2 ± 2.5
S. rolfsii	47.7 ± 4.8	56.3 ± 5.2

* Values are the average of three independent tests. ± Standard deviation.

Table 2 Percentage inhibition of mycelial growth of phytopathogenic fungi by VOC production of *Bacillus* strains in overlapping plate tests

The inhibitory and antifungal activity of *B. subtilis* strains against fungi of agricultural interest by volatile compounds has been reported previously, Chaurasia *et al*. (2005) show 60-65% inhibitory activities of *B. subtilis* (NRRL B-30408) on *A. alternata* and *F. oxysporum*. Furthermore, Zhao *et al*. (2019) reported the inhibitory capacity of agriculturally important fungi by *B. subtilis* CF-3 where (S)-1-octanol, benzoic acid, 2,4-di-ter¬-butylthiophenol, benzaldehyde and benzothiazole were the key compounds for the inhibition of *C. gloesporoides* and *M. fructicola.*

In contrast to lipopeptides, the mechanism of inhibition of *Bacillus* spp. VOCs is unclear, however, it is known that they can inhibit conidial germination and morphologically affect the hyphae of pathogenic fungi (Zhang *et al*., 2020), it has also been reported that VOCs from *B. subtilis* modify the regulation of gene expression related to cell membrane fluidity, cell wall integrity, energy metabolism and cell wall degrading enzyme production (Wang *et al*., 2021).

ISSN: 2410-3462

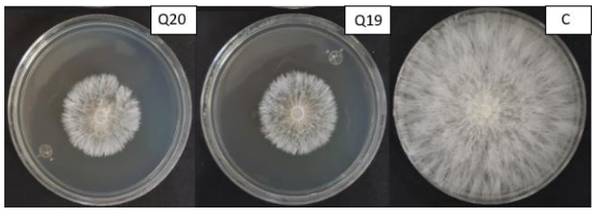

Figure 3. Inhibition of mycelial growth of *S. rolfsii* by strains Q20 and Q19 in overlapping plate assays, control (C).

Acknowledgements

This work was funded by the Secretariat of University Services and Liaison of the UAQ, through the Fund for the Development of Knowledge (FONDEC). Project registration number SVSU-DV-2022-022.

Conclusions

The study strains *B. licheniformis* Q19 and *B. subtilis* Q20 show in vitro biocontrol activity on phytopathogenic fungi affecting fruit and vegetable crops. *Alternaria alternata* was the fungus that was mostly inhibited by the production of lipopeptides from Q20 and by volatile compounds produced by Q19.

References

Abdallah, M., De Boevre, M., Landschoot, S., De Saeger, S., Haesaert, G., & Audenaert, K. (2018). Fungal endophytes control *Fusarium graminearum* and reduce trichothecenes and zearalenone in maize. *Toxins*, 10(12), 493. https://doi.org/10.3390/toxins10120493

Baldivia, A. S., & Ibarra, G. R. (2017). La disponibilidad de alimentos en méxico: Un análisis de la producción agrícola de 35 años y su proyección para 2050. *Papeles de Poblacion*, 23(93), 207–230. https://doi.org/10.22185/24487147.2017.93.027

Baysal, O., Lai, D., Xu, H.-H., Siragusa, M., Carimi, F., Teixeira Da Silva, J. A., & Tö, M. (2013). A proteomic approach provides new insights into the control of soil-borne plant pathogens by *Bacillus* species. *PLoS ONE*, 8(1), https://doi.org/10.1371/journal.pone.0053182

Benkeblia, N., Tennant, D. P. F., Jawandha, S. K., & Gill, P. S. (2011). Preharvest and harvest factors influencing the postharvest quality of tropical and subtropical fruits. *Postharvest Biology and Technology of Tropical and Subtropical Fruits*, 1, 112-142e. https://doi.org/10.1533/9780857093622.112

Chaurasia, B., Pandey, A., Palni, L. M. S., Trivedi, P., Kumar, B., & Colvin, N. (2005). Diffusible and volatile compounds produced by an antagonistic *Bacillus subtilis* strain cause structural deformations in pathogenic fungi in vitro. *Microbiological Research*, 160(1), 75–81. https://doi.org/10.1016/j.micres.2004.09.013

Dimkić, I., Živković, S., Berić, T., Ivanović, Ž., Gavrilović, V., Stanković, S., & Fira, D. (2013). Characterization and evaluation of two *Bacillus* strains, SS-12.6 and SS-13.1, as potential agents for the control of phytopathogenic bacteria and fungi. *Biological Control*, 65(3), 312–321. https://doi.org/10.1016/j.biocontrol.2013.03.012

Ezziyyani, M., Sánchez, C. P., Requena, M. E., Rubio, L. & Castillo, M. E. C. (2004). Biocontrol por "*Streptomyces rochei*" - Ziyani -, de la podredumbre del pimiento ("*Capsicum annuum* L.") causada por "*Phytophthora capsici*" In Anales de Biología, 26, 69-78. Servicio de Publicaciones de la Universidad de Murcia. Consultado el 25 de dicimebre de 2022 de https://www.um.es/analesdebiologia/numeros/26/PDF/08-BIOCONTROL.pdf

Köhl, J., Kolnaar, R., & Ravensberg, W. J. (2019). Mode of action of microbial biological control agents against plant diseases: Relevance beyond efficacy. *Frontiers in Plant Science*, 10, 1–19. https://doi.org/10.3389/fpls.2019.00845

Nasir, M. N., & Besson, F. (2012). Interactions of the antifungal mycosubtilin with ergosterol-containing interfacial monolayers. *Biochimica et Biophysica Acta - Biomembranes*, *1818*(5), 1302–1308. https://doi.org/10.1016/j.bbamem.2012.01.020

Oda, M., Takahashi, M., Matsuno, T., Uoo, K., Nagahama, M., & Sakurai, J. (2010). Hemolysis induced by *Bacillus cereus* sphingomyelinase. *Biochimica et Biophysica Acta (BBA) - Biomembranes*, *1798*(6), 1073–1080. https://doi.org/10.1016/j.bbamem.2010.03.004

Ongena, M., & Jacques, P. (2008). *Bacillus* lipopeptides: versatile weapons for plant disease biocontrol. *Trends in Microbiology*, 16(3), 115–125. https://doi.org/10.1016/j.tim.2007.12.009

Pan, X., Chen, X., Su, X., Feng, Y., Tao, Y., & Dong, Z. (2014). Involvement of SpoVG in hemolysis caused by *Bacillus subtilis*. *Biochemical and Biophysical Research Communications*, *443*(3), 899–904. https://doi.org/10.1016/j.bbrc.2013.12.069

Płaza, G., Chojniak, J., Rudnicka, K., Paraszkiewicz, K., & Bernat, P. (2015). Detection of biosurfactants in *Bacillus* species: genes and products identification. *Journal of Applied Microbiology*, 119(4), 1023–1034. https://doi.org/10.1111/jam.12893

Qi, G., Zhu, F., Du, P., Yang, X., Qiu, D., Yu, Z., Chen, J., & Zhao, X. (2010). Lipopeptide induces apoptosis in fungal cells by a mitochondria-dependent pathway. *Peptides*, 31(11), 1978–1986. https://doi.org/10.1016/j.peptides.2010.08.003

Rodríguez-Chávez, J. L., Juárez-Campusano, Y. S., Delgado, G., & Pacheco Aguilar, J. R. (2019). Identification of lipopeptides from *Bacillus* strain Q11 with ability to inhibit the germination of *Penicillium expansum*, the etiological agent of postharvest blue mold disease. *Postharvest Biology and Technology*, 155, 72–79. https://doi.org/10.1016/j.postharvbio.2019.05.011

Romano, A., Vitullo, D., Senatore, M., Lima, G., & Lanzotti, V. (2013). Antifungal cyclic lipopeptides from *Bacillus amyloliquefaciens* strain BO5A. *Journal of Natural Products*, 76(11), 2019–2025. https://doi.org/10.1021/np400119n

Ruiz, E., Mejía, M., Cristóbal, J., Valencia, A., & Reyes, A. (2014). Actividad antagónica de filtrados de *Bacillus subtilis* contra *Colletotrichum gloeosporioides*. *Revista Mexicana de Ciencias Agrícolas*, 5(7), 1325–1332. Consultado el 25 de diciembre de 2022 en https://www.scielo.org.mx/pdf/remexca/v5n7/v5n7a15.pdf.

Sarwar, A., Brader, G., Corretto, E., Aleti, G., Ullah, M. A., Sessitsch, A., & Hafeez, F. Y. (2018). Qualitative analysis of biosurfactants from *Bacillus* species exhibiting antifungal activity. *PloS One*, 13(6), https://doi.org/10.1371/journal.pone.0198107

Shrivastava, P., Kumar, R., & Yandigeri, M. S. (2017). *In vitro* biocontrol activity of halotolerant *Streptomyces aureofaciens* K20: A potent antagonist against Macrophomina phaseolina (Tassi) Goid. *Saudi Journal of Biological Sciences*, 24(1), 192–199. https://doi.org/10.1016/j.sjbs.2015.12.004

SIAP. (2021). El SIAP presenta: Expectativas agroalimentarias 2021. Consultado el 20 de diciembre de 2022, de https://www.gob.mx/siap/es/articulos/el-siap-presenta-expectativas-agroalimentarias-2021?idiom=es

Steinborn, G., Hajirezaei, M., & Hofemeister, J. (2005). Bac genes for recombinant bacilysin and anticapsin production in *Bacillus* host strains. *Archives of Microbiology*, 183(2), 71–79. https://doi.org/10.1007/s00203-004-0743-8

Sułowicz, S., & Piotrowska, Z. (2016). The impact of fungicides on soil microorganisms. *Postępy Mikrobiologii*, 55, 12–18. Consultado el 25 de diciembre del 2022, de https://www.researchgate.net/publication/299615676_The_impact_of_fungicides_on_soil_microorganisms.

Villarreal, M., Villa, E., Cira, L., Estrada, M., Parra, F., & De los Santos, S. (2018). El género *Bacillus* como agente de control biológico y sus implicaciones en la bioseguridad agrícola. *Revista Mexicana de Fitopatología*, 36(1), 95–130. https://doi.org/10.18781/r.mex.fit.1706-5

Vlot, C., & Rosenkranz, M. (2022). Volatile compounds—the language of all kingdoms? *Journal of Experimental Botany*, 73, 445–448. https://doi.org/10.1093/jxb/erab528

Wang, K., Qin, Z., Wu, S., Zhao, P., Zhen, C., & Gao, H. (2021). Antifungal Mechanism of Volatile Organic Compounds Produced by *Bacillus subtilis* CF-3 on *Colletotrichum gloeosporioides* Assessed Using Omics Technology. *Journal of Agricultural and Food Chemistry*, *69*(17), 5267–5278. https://doi.org/10.1021/acs.jafc.1c00640

ISSN: 2410-3462

Wang, Y., Zhang, C., Liang, J., Wu, L., Gao, W., & Jiang, J. (2020). Iturin A extracted from *Bacillus subtilis* WL-2 affects *Phytophthora infestans* via cell structure disruption, oxidative stress, and energy supply dysfunction. *Frontiers in Microbiology*, 11, 1–12. https://doi.org/10.3389/fmicb.2020.536083

Yahaya, S. M., & Mardiyya, A. Y. (2019). Review of post-harvest losses of fruits and vegetables. *Biomedical Journal of Scientific & Technical Research*, 13(4), 10192–10200. https://doi.org/10.26717/bjstr.2019.13.002448

Yu, D., Fang, Y., Tang, C., Klosterman, S. J., Tian, C., & Wang, Y. (2019). Genomewide transcriptome profiles reveal how *Bacillus subtilis* lipopeptides inhibit microsclerotia formation in *Verticillium dahliae*. *Molecular Plant-Microbe Interactions*, *32*(5), 622–634. https://doi.org/10.1094/MPMI-08-18-0233-R

Yuan, J., Raza, W., Shen, Q., & Huang, Q. (2012). Antifungal activity of *Bacillus amyloliquefaciens* NJN-6 volatile compounds against *Fusarium oxysporum* f. sp. cubense. *Applied and Environmental Microbiology*, 78, 5942–5944. https://doi.org/10.1128/AEM.01357-12

Zhang, D., Qiang, R., Zhou, Z., Pan, Y., Yu, S., Yuan, W., Cheng, J., Wang, J., Zhao, D., Zhu, J., & Yang, Z. (2022). Biocontrol and action mechanism of *Bacillus subtilis* lipopeptides' fengycins against *Alternaria solani* in potato as assessed by a transcriptome analysis. *Frontiers in Microbiology*, *13*(May). https://doi.org/10.3389/fmicb.2022.861113

Zhang, D., Yu, S., Yang, Y., Zhang, J., Zhao, D., Pan, Y., Fan, S., Yang, Z., & Zhu, J. (2020). Antifungal effects of volatiles produced by *Bacillus subtilis* against *Alternaria solani* in potato. *Frontiers in Microbiology*, 11, 1–12. https://doi.org/10.3389/fmicb.2020.01196

Zhao, P., Li, P., Wu, S., Zhou, M., Zhi, R., & Gao, H. (2019). Volatile organic compounds (VOCs) from *Bacillus subtilis* CF-3 reduce anthracnose and elicit active defense responses in harvested litchi fruits. *AMB Express*, *9*(1). https://doi.org/10.1186/s13568-019-0841-2

Zhao, X., Han, Y., Tan, X. qian, Wang, J., & Zhou, Z. jiang. (2014). Optimization of antifungal lipopeptide production from *Bacillus* sp. BH072 by response surface methodology. *Journal of Microbiology*, 52(4), 324–332. https://doi.org/10.1007/s12275-014-3354-3

ISSN: 2410-3462

[Title in Times New Roman and Bold No. 14 in English and Spanish]

Surname (IN UPPERCASE), Name 1st Author†*, Surname (IN UPPERCASE), Name 1st Coauthor, Surname (IN UPPERCASE), Name 2nd Coauthor and Surname (IN UPPERCASE), Name 3rd Coauthor

Institutional Affiliation of Author including Dependency (No.10 Times New Roman and Italic)

International Identification of Science - Technology and Innovation

ID 1st Author: (ORC ID - Researcher ID Thomson, arXiv Author ID - PubMed Author ID - Open ID) and CVU 1st author: (Scholar-PNPC or SNI-CONACYT) (No.10 Times New Roman)

ID 1st Coauthor: (ORC ID - Researcher ID Thomson, arXiv Author ID - PubMed Author ID - Open ID) and CVU 1st coauthor: (Scholar or SNI) (No.10 Times New Roman)

ID 2nd Coauthor: (ORC ID - Researcher ID Thomson, arXiv Author ID - PubMed Author ID - Open ID) and CVU 2nd coauthor: (Scholar or SNI) (No.10 Times New Roman)

ID 3rd Coauthor: (ORC ID - Researcher ID Thomson, arXiv Author ID - PubMed Author ID - Open ID) and CVU 3rd coauthor: (Scholar or SNI) (No.10 Times New Roman)

(Report Submission Date: Month, Day, and Year); Accepted (Insert date of Acceptance: Use Only ECORFAN)

Abstract (In English, 150-200 words)

Objectives
Methodology
Contribution

Abstract (In Spanish, 150-200 words)

Objectives
Methodology
Contribution

Keywords (In English)

Indicate 3 keywords in Times New Roman and Bold No. 10

Keywords (In Spanish)

Indicate 3 keywords in Times New Roman and Bold No. 10

Citation: Surname (IN UPPERCASE), Name 1st Author, Surname (IN UPPERCASE), Name 1st Coauthor, Surname (IN UPPERCASE), Name 2nd Coauthor and Surname (IN UPPERCASE), Name 3rd Coauthor. Paper Title. Journal Simulation and Laboratory. Year 1-1: 1-11 [Times New Roman No.10]

* Correspondence to Author (example@example.org)
† Researcher contributing as first author.

Introduction

Text in Times New Roman No.12, single space.

General explanation of the subject and explain why it is important.

What is your added value with respect to other techniques?

Clearly focus each of its features

Clearly explain the problem to be solved and the central hypothesis.

Explanation of sections Article.

Development of headings and subheadings of the article with subsequent numbers

[Title No.12 in Times New Roman, single spaced and bold]

Products in development No.12 Times New Roman, single spaced.

Including graphs, figures and tables-Editable

In the article content any graphic, table and figure should be editable formats that can change size, type and number of letter, for the purposes of edition, these must be high quality, not pixelated and should be noticeable even reducing image scale.

[Indicating the title at the bottom with No.10 and Times New Roman Bold]

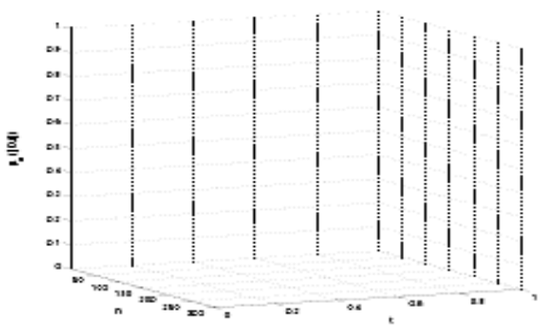

Graphic 1 Title and *Source (in italics)*

Should not be images-everything must be editable.

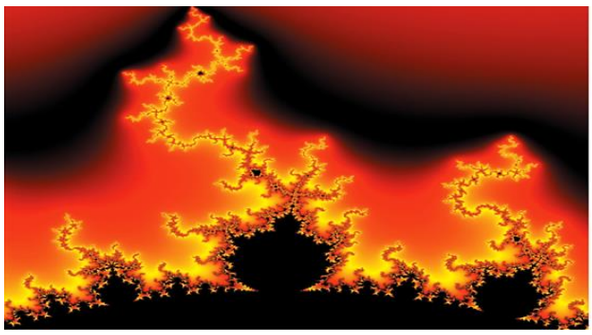

Figure 1 Title and *Source (in italics)*

Should not be images-everything must be editable.

Table 1 Title and *Source (in italics)*

Should not be images-everything must be editable.

Each article shall present separately in **3 folders**: a) Figures, b) Charts and c) Tables in .JPG format, indicating the number and sequential Bold Title.

For the use of equations, noted as follows:

$$Y_{ij} = \alpha + \sum_{h=1}^{r} \beta_h X_{hij} + u_j + e_{ij} \qquad (1)$$

Must be editable and number aligned on the right side.

Methodology

Develop give the meaning of the variables in linear writing and important is the comparison of the used criteria.

Results

The results shall be by section of the article.

Annexes

Tables and adequate sources

Thanks

Indicate if they were financed by any institution, University or company.

Conclusions

Explain clearly the results and possibilities of improvement.

ISSN 2410-3462

References

Use APA system. Should not be numbered, nor with bullets, however if necessary numbering will be because reference or mention is made somewhere in the Article.

Use Roman Alphabet, all references you have used must be in the Roman Alphabet, even if you have quoted an Article, book in any of the official languages of the United Nations (English, French, German, Chinese, Russian, Portuguese, Italian, Spanish, Arabic), you must write the reference in Roman script and not in any of the official languages.

Technical Specifications

Each article must submit your dates into a Word document (.docx):

Journal Name
Article title
Abstract
Keywords
Article sections, for example:

1. Introduction
2. Description of the method
3. Analysis from the regression demand curve
4. Results
5. Thanks
6. Conclusions
7. References

Author Name (s)
Email Correspondence to Author
References

Intellectual Property Requirements for editing:

-Authentic Signature in Color of Originality Format Author and Coauthors

-Authentic Signature in Color of the Acceptance Format of Author and Coauthors

-Authentic Signature in Color of the Conflict of Interest Format of Author and Co-authors

ISSN 2410-3462

Reservation to Editorial Policy

Journal Simulation and Laboratory reserves the right to make editorial changes required to adapt the Articles to the Editorial Policy of the Research Journal. Once the Article is accepted in its final version, the Research Journal will send the author the proofs for review. ECORFAN® will only accept the correction of errata and errors or omissions arising from the editing process of the Research Journal, reserving in full the copyrights and content dissemination. No deletions, substitutions or additions that alter the formation of the Article will be accepted.

Code of Ethics - Good Practices and Declaration of Solution to Editorial Conflicts

Declaration of Originality and unpublished character of the Article, of Authors, on the obtaining of data and interpretation of results, Acknowledgments, Conflict of interests, Assignment of rights and Distribution

The ECORFAN-Mexico, S.C Management claims to Authors of Articles that its content must be original, unpublished and of Scientific, Technological and Innovation content to be submitted for evaluation.

The Authors signing the Article must be the same that have contributed to its conception, realization and development, as well as obtaining the data, interpreting the results, drafting and reviewing it. The Corresponding Author of the proposed Article will request the form that follows.

Article title:

- The sending of an Article to Journal Simulation and Laboratory emanates the commitment of the author not to submit it simultaneously to the consideration of other series publications for it must complement the Format of Originality for its Article, unless it is rejected by the Arbitration Committee, it may be withdrawn.

- None of the data presented in this article has been plagiarized or invented. The original data are clearly distinguished from those already published. And it is known of the test in PLAGSCAN if a level of plagiarism is detected Positive will not proceed to arbitrate.

- References are cited on which the information contained in the Article is based, as well as theories and data from other previously published Articles.

- The authors sign the Format of Authorization for their Article to be disseminated by means that ECORFAN-Mexico, S.C. In its Holding Bolivia considers pertinent for disclosure and diffusion of its Article its Rights of Work.

- Consent has been obtained from those who have contributed unpublished data obtained through verbal or written communication, and such communication and Authorship are adequately identified.

- The Author and Co-Authors who sign this work have participated in its planning, design and execution, as well as in the interpretation of the results. They also critically reviewed the paper, approved its final version and agreed with its publication.

- No signature responsible for the work has been omitted and the criteria of Scientific Authorization are satisfied.

- The results of this Article have been interpreted objectively. Any results contrary to the point of view of those who sign are exposed and discussed in the Article.

Copyright and Access

The publication of this Article supposes the transfer of the copyright to ECORFAN-Mexico, SC in its Holding Bolivia for it Journal Simulation and Laboratory, which reserves the right to distribute on the Web the published version of the Article and the making available of the Article in This format supposes for its Authors the fulfilment of what is established in the Law of Science and Technology of the United Mexican States, regarding the obligation to allow access to the results of Scientific Research.

Article Title:

Name and Surnames of the Contact Author and the Coauthors	Signature
1.	
2.	
3.	
4.	

Principles of Ethics and Declaration of Solution to Editorial Conflicts

Editor Responsibilities

The Publisher undertakes to guarantee the confidentiality of the evaluation process, it may not disclose to the Arbitrators the identity of the Authors, nor may it reveal the identity of the Arbitrators at any time.

The Editor assumes the responsibility to properly inform the Author of the stage of the editorial process in which the text is sent, as well as the resolutions of Double-Blind Review.

The Editor should evaluate manuscripts and their intellectual content without distinction of race, gender, sexual orientation, religious beliefs, ethnicity, nationality, or the political philosophy of the Authors.

The Editor and his editing team of ECORFAN® Holdings will not disclose any information about Articles submitted to anyone other than the corresponding Author.

The Editor should make fair and impartial decisions and ensure a fair Double-Blind Review.

Responsibilities of the Editorial Board

The description of the peer review processes is made known by the Editorial Board in order that the Authors know what the evaluation criteria are and will always be willing to justify any controversy in the evaluation process. In case of Plagiarism Detection to the Article the Committee notifies the Authors for Violation to the Right of Scientific, Technological and Innovation Authorization.

Responsibilities of the Arbitration Committee

The Arbitrators undertake to notify about any unethical conduct by the Authors and to indicate all the information that may be reason to reject the publication of the Articles. In addition, they must undertake to keep confidential information related to the Articles they evaluate.

Any manuscript received for your arbitration must be treated as confidential, should not be displayed or discussed with other experts, except with the permission of the Editor.

The Arbitrators must be conducted objectively, any personal criticism of the Author is inappropriate.

The Arbitrators must express their points of view with clarity and with valid arguments that contribute to the Scientific, Technological and Innovation of the Author.

The Arbitrators should not evaluate manuscripts in which they have conflicts of interest and have been notified to the Editor before submitting the Article for Double-Blind Review.

Responsibilities of the Authors

Authors must guarantee that their articles are the product of their original work and that the data has been obtained ethically.

Authors must ensure that they have not been previously published or that they are not considered in another serial publication.

Authors must strictly follow the rules for the publication of Defined Articles by the Editorial Board.

The authors have requested that the text in all its forms be an unethical editorial behavior and is unacceptable, consequently, any manuscript that incurs in plagiarism is eliminated and not considered for publication.

Authors should cite publications that have been influential in the nature of the Article submitted to arbitration.

Information services

Indexation - Bases and Repositories

RESEARCH GATE (Germany)
GOOGLE SCHOLAR (Citation indices-Google)
REDIB (Ibero-American Network of Innovation and Scientific Knowledge- CSIC)
MENDELEY (Bibliographic References Manager)
DULCINEA (Spanish scientific journals)
UNIVERSIA (University Library-Madrid)
SHERPA (University of Nottingham - England)

Publishing Services

Citation and Index Identification H
Management of Originality Format and Authorization
Testing Article with PLAGSCAN
Article Evaluation
Certificate of Double-Blind Review
Article Edition
Web layout
Indexing and Repository
ArticleTranslation
Article Publication
Certificate of Article
Service Billing

Editorial Policy and Management

21 Santa Lucía, CP-5220. Libertadores -Sucre – Bolivia. Phones: +52 1 55 6159 2296, +52 1 55 1260 0355, +52 1 55 6034 9181; Email: contact@ecorfan.org www.ecorfan.org

Journal Simulation and Laboratory

2410 3462
ISSN 2410 - 3462

www.ecorfan.org